Time-resolved optical transients in tetragonal $BaTiO_3$

Mike Melnichuk and Lowell T. Wood

Department of Physics, University of Houston, Houston, Texas 77204-5005

We present and analyze the room temperature ($T=23.5\,^{\circ}C$) time behavior of the transmitted intensities of polarized light passing through an unclamped (100)-type single crystal of barium titanate ($BaTiO_3$) when subject to a time-dependent, externally applied electric field. To the authors' knowledge, this is the first reported observation and analysis of such time-resolved optical transients. According to a previous [J. Opt. Soc. Am. A **22**, 377 (2005)] observation by the authors, this original optical technique can, in principle, be used on 18 out of 20 noncentrosymmetric crystal point groups where the first-order (Pockels) and second-order (Kerr) electro-optic effects coexist. Because of its nondestructive nature, this novel optical method would be a useful tool in other fields of condensed-matter physics in which time-behavior observation and characterization of certain physical parameters of crystals are important.

OCIS codes: 190.3270, 160.2260, 260.1180, 160.1190, 230.4110.

1. INTRODUCTION

When an external electric field is applied to a ferroelectric sample of tetragonal $BaTiO_3$, the indices of refraction undergo changes as a result of the electro-optic effect. If light shines on the sample, these variations in the refractive indices induce detectable changes in the transmitted intensity of the light. These intensity changes are a function of the state of polarization of the transmitted light. By measuring and analyzing the variation of the polarized light intensity for different values of the applied electric fields, it is possible to obtain quantitative information about some of the electro-optic coefficients of the ferroelectric crystal. Results from these measurements were reported by the authors in a previous paper[1] in which they determined the two off-diagonal Kerr coefficients for an unclamped bulk single crystal of $BaTiO_3$ at room temperature ($T=23.5\,^{\circ}C$) and a light wavelength $\lambda=632.8$ nm.

Here we concentrate on the time behavior of the transmitted light intensity during three main transitions in the $BaTiO_3$ crystal, all of which are induced by abrupt changes in the externally applied electric field. The first main type of transient (excitation) in the light intensity occurs when the electric field across the $BaTiO_3$ sample changes sharply from zero to a nonzero value. The second main type of optical transient (switching) occurs when the direction of the voltage across the sample, having a nonzero value, is suddenly inverted. The third type of transient behavior (relaxation) occurs when the electric circuit is opened and the crystal starts to relax back to its original unexcited state.

By analyzing and theoretically modeling these time-resolved optical transients, we were able to deduce quantitative and qualitative information with regard to the excitation, switching, and relaxation-time behavior of the ordinary (n_o) and extraordinary (n_e) indices of refraction for a (100) bulk single crystal of tetragonal $BaTiO_3$ when subject to an abruptly changing applied electric potential.

We proceed in the following manner. First we will show these optical transients and provide a detailed explanation of the way they were experimentally measured. Then we will construct a theoretical model of the transients and compare that model with our experimental results.

2. EXPERIMENT AND RESULTS

We begin by providing a view of the experimental data; then we go on to describe in detail the layout of the experiment. In Subsection 2.B we return to the experimental results and explain the collection procedure.

A. Experimental Design

A simplified version of the experiment is presented in Fig. 1. The modulated optical intensities I_y' and I_z' along the y' and z' directions have their polarizations orthogonal relative to each other. The Cartesian system of coordinates (x,y',z') is rotated with respect to the Cartesian coordinate system (x,y,z) by an angle $\theta=15°$ in the trigonometric direction. The time evolution of I_y' and I_z' for different electric fields is shown in Figs. 2 and 3 during two experimental trials. The I_m is a fraction of the intensity of the incident beam and is used in the experiment for monitoring purposes only. By analyzing the behavior of the two modulated intensities mentioned above, we will be able to extract quantitative information regarding the time constants associated with the excitation, switching, and relaxation processes induced in our ferroelectric sample by changes in the externally applied electric field.

The actual experimental layout used for collecting the above mentioned data is presented in detail in Fig. 4. The experiment was performed at a temperature of $23.5\,^{\circ}C$. The sample was an unclamped, 5-mm×5-mm×1-mm, two-face-polished, (100)-oriented, single crystal of $BaTiO_3$. It was mounted with the spontaneous polarization $\mathbf{P}_s$ in the z direction. A pair of electrodes 3 mm in diameter was created by sputtering a 20-nm-thick layer of gold on the 5-mm×5-mm opposite faces of the sample. The connection between these electrodes and the electrical cables from a high-voltage power supply (PS) was made through a pair of thin gold wires (GW) which were

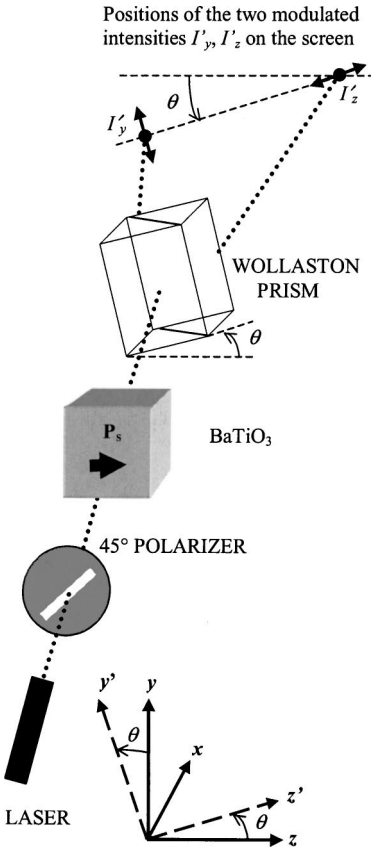

Fig. 1. Simple schematic of the optical amplitude modulation system. The modulated optical intensities I_y' and I_z' are polarized along the axes y' and z', respectively.

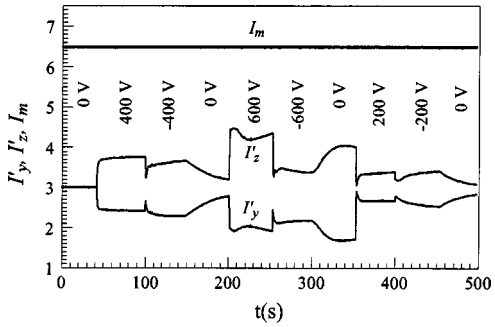

Fig. 2. Time-behavior plot of the two modulated orthogonal intensities I_y',I_z' and the monitoring intensity I_m for the first experimental trial. I_y' and I_z' are polarized along the axes y' and z', respectively. The Cartesian system of coordinates (x,y',z') is rotated counterclockwise by an angle $\theta=15°$ relative to the Cartesian coordinate system (x,y,z). The applied electric field (E_1) across the $BaTiO_3$ sample was switched in a steplike fashion approximately every 50 s for 500 s. The values in volts of the electric field taken in chronological order were 0, +400, −400, 0, +600, −600, 0, +200, −200, 0.

permanently attached to the sample electrodes with a colloidal silver paste solution. The front surface of the $BaTiO_3$ crystal was illuminated with an incandescent lamp (IL), making it visible to a CCD camera (BASLER A101p; 1300H × 1030V pixels; pixel size, 6.7 μm × 6.7 μm).

A 0.5-mW He–Ne laser beam of wavelength λ = 632.8 nm and diameter 0.48 mm at the $1/e^2$ points transmitted through the crystal after being split by a beam splitter (BS1). One part of the incident beam went into a light-intensity detector (D1), which was used to monitor changes in the magnitude of the incident beam intensity. Before reaching the crystal, the incoming light was linearly polarized at 45° relative to $\mathbf{P}_s$ by a polarizer (PO). After passing through the crystal, the transmitted

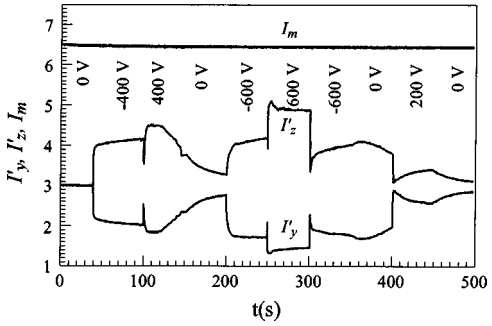

Fig. 3. Same as Fig. 2 but for the second experimental trial. The values in volts of the electric field taken in chronological order were: 0, −400, +400, 0, −600, +600, −600, 0, +200, 0. In this case the −400-V field on the sample was kept on for ≈20 s only.

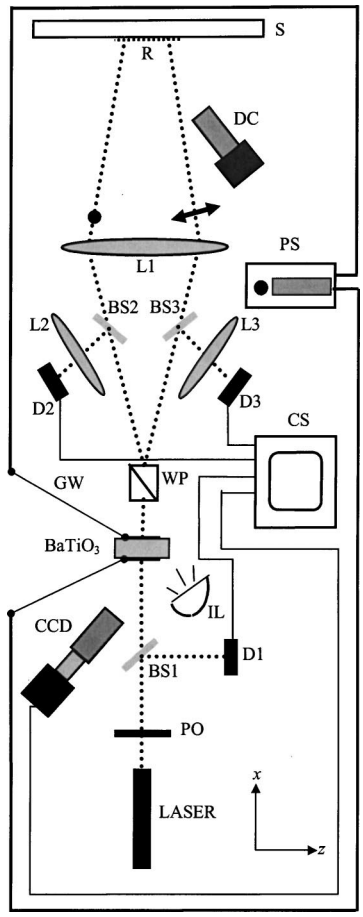

Fig. 4. Schematic of the experimental setup; the y axis points out of the paper. The setup contains the following elements: laser, $BaTiO_3$ crystal, 45°-linear polarizer (PO), Wollaston prism (WP), beam splitters (BS1, BS2, BS3), intensity detectors (D1, D2, D3), convergent lenses (L1, L2, L3), CCD camera (CCD), digital camera (DC), computer system (CS), incandescent lamp (IC), power supply (PS), millimeter ruler (R), screen (S), and a pair of gold wires (GW).

beam was divided with a Wollaston prism (WP) into two beams of light having mutually perpendicular polarizations. The prism was rotated counterclockwise by an angle $\theta = 15°$ in the plane normal to the direction x of light propagation (see Fig. 1). The rotated Wollaston prism was the novel design feature that differentiated our amplitude modulator from the standard ones found in the optical literature[2–13] because it allowed modulation of both orthogonally polarized waves at the same time.

Each of those two orthogonally polarized beams was then further separated into two lower-intensity beams by a set of beam splitters (BS2, BS3). For each of these new lower-intensity beams, part was focused by a convergent lens (L2 or L3) into a light-intensity detector (D2 or D3) while the other part was passed through a common convergent lens (L1) onto a screen (S) having a thin, millimeter ruler (R) attached to it.

B. Experimental Results

Figures 2 and 3 show the time evolution of the optical intensities measured by the three detectors (D1, D2, D3), for two experimental trials. During each of these trials, the electric field across the sample was varied in a steplike fashion at intervals of ≈50 s for 500 s; this was done manually for positive, zero, and negative values of the electrical potential by a toggle switch. Intensity values were acquired every 0.02 s for 500 s with the data-collection software, (Vernier LabPro 2.2.1.); detector D1 measured the monitoring beam intensity (I_m), D2 the intensity polarized along the y' axis (I_y'), and D3 the intensity polarized along the z' axis (I_z'). These three intensity values were plotted versus time with the software PSI-Plot (Version 7). The optical transients manifest themselves as sharp and obvious changes in the two polarized intensities each time the electric field across the $BaTiO_3$ sample suddenly takes on a value that is different in magnitude or direction from the previous one.

The CCD camera acquired images of the crystal's surface once per second for 500 s, while pictures of the transmitted light's intensity patterns on the screen were taken manually approximately every 25 s for 500 s with a Sony digital camera (DC) having the specifications XGA, 1024 × 768 pixels. The CCD camera was used to monitor changes at the crystal's surface, while the digital camera was employed for capturing any change in the intensity pattern of light when the external electric field was varied across the sample. All the experimental data were acquired and processed with a computer system (CS).

3. THEORETICAL MODELS

Each of the three types of time-resolved transients presented in Subsection 2.B will be the subject of a corresponding theoretical model; this will be done in two parts. Subsection 3.A will be devoted to finding the expressions for the time-dependent electric potentials across the sample in all three of the situations. In Subsection 3.B we will concentrate on integrating the formulas for these potentials with the electro-optic expressions for the modulated light intensities transmitted through the crystal. In doing that, we will be able to extract some room-temperature quantitative information regarding the excitation, switching, and relaxation time constants for the indices of refraction of $BaTiO_3$ from the time behavior of those transmission intensities.

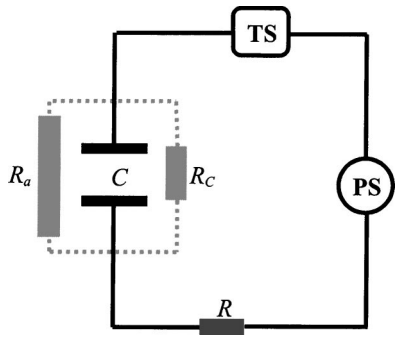

Fig. 5. Schematic of the electric circuit; only the solid line represents real electric cable. The circuit comprises the following elements: power supply (PS), toggle switch (TS), equivalent resistance of wire circuit (R), $BaTiO_3$ capacitor (C) with its internal resistance (R_C), and the equivalent resistance of the ambient medium (R_a).

A. Voltage Models

The electric circuit containing the $BaTiO_3$ sample can be modeled in a general RC circuit as shown in Fig. 5. The $BaTiO_3$ sample with its electrodes acts as a capacitor of capacitance C. R stands for the equivalent resistance of the wire circuit, R_C is the internal resistance of the capacitor, R_a is the resistance of the ambient medium surrounding the capacitor, and TS represents the electric toggle switch. The two circuits in parallel with the capacitor are represented by dotted lines because they do not represent standard circuits in which charge conduction occurs through an electrical conductor but rather circuits through the two different media connecting the capacitor's plates. One of these media (between the plates) is the actual ferroelectric in which some conduction occurs because $BaTiO_3$ is not a perfect dielectric; the other medium is the ambient air. The decrease in the capacitor's charge Q through these two charge-loss media weakens the voltage drop V_C across the capacitor. The charge leakage processes in the two media can be modeled as two electrical circuits in parallel with the capacitor, each having different resistances R_C and R_a. It is realistic to assume $R_a \gg R_C$, because it takes much longer for the capacitor to discharge through the ambient air than through the ferroelectric dielectric between its plates.[14–17]

When a potential difference from the power supply $V(t)$ is applied across the sample, the time-dependent voltage $V_C(t)$ across the capacitor can be deduced from the following set of equations:

$$V_C(t) + i(t)R = V(t), \tag{1}$$

$$i(t) - \frac{V_C(t)}{R_C} - \frac{V_C(t)}{R_a} = \frac{dQ(t)}{dt}, \tag{2}$$

$$Q(t) = CV_C(t), \tag{3}$$

which lead to a nonhomogeneous linear differential equation for the capacitor's voltage:

$$\frac{dV_C}{dt} + \frac{1}{C}\left(\frac{1}{R} + \frac{1}{R_C} + \frac{1}{R_a}\right)V_C = \frac{1}{CR}V. \tag{4}$$

The general solution of this equation as a function of time has the form

$$V_C(t) = V_C(t_0)\exp\left[-\frac{(t-t_o)}{\tau}\right] + \frac{1}{RC}\int_{t_0}^{t} V(t')\exp\left[-\frac{(t-t')}{\tau}\right]dt' \tag{5}$$

with the time constant

$$\tau = \frac{C}{1/R + 1/R_C + 1/R_a}. \tag{6}$$

Here $i(t)$ is the instantaneous conduction current through the wire circuit, and $t_0 \leqslant t' \leqslant t$, with t_0 the moment when the voltage of the power supply is changed. To obtain the explicit solution of Eq. (4) we had to assume that the capacitance C is not dependent on the voltage V_C across the capacitor. This is a risky assumption considering that we are actually dealing with a capacitor containing a nonlinear dielectric. However, considering that assumption, our solution [Eq. (5)] has the advantage of taking into account the conduction of charge through the dielectric and the ambient air, making it more general than the standard solution for a time-invariant RC circuit found in the literature on electrical circuits.[18] It is this solution that we employ in modeling the three types of transients specified in Section 1.

In the first type of transient, the voltage abruptly changes from zero to a nonzero value, $V_C(t_0)=0$ V to $V(t')=V$ (constant) for $t_0 \leqslant t' \leqslant t$. According to Eq. (5), the voltage across the capacitor for this case takes the form

$$V_C(t) = \frac{\tau}{RC}V\left\{1 - \exp\left[-\frac{(t-t_o)}{\tau}\right]\right\}. \tag{7}$$

This formula describes the charging process of a real capacitor with a dielectric between its plates. For an ideal capacitor, $R_a, R_C \gg R$ and

$$\tau \cong \tau_e = RC, \tag{8}$$

resulting in the well-known formula for capacitor charging that is derived in most textbooks,

$$V_C(t) \cong V\left\{1 - \exp\left[-\frac{(t-t_o)}{\tau_e}\right]\right\}, \tag{9}$$

where τ_e stands for the capacitor's excitation time constant.

For the second type of transient, the nonzero voltage of the power supply is suddenly inverted ($-V$). Assuming that the capacitor was fully charged by the time the voltage was reversed, Eq. (5) becomes

$$V_C(t) = -\frac{\tau}{RC}V\left\{1 - 2\exp\left[-\frac{(t-t_o)}{\tau}\right]\right\}, \tag{10}$$

where t_0 represents the moment when the voltage of the power supply was inverted.

For an ideal capacitor Eq. (10) is approximated by

$$V_C(t) \cong -V\left\{1 - 2\exp\left[-\frac{(t-t_o)}{\tau_s}\right]\right\}, \tag{11}$$

with the switching time constant τ_s having the same approximate form as τ_e above.

The third transient observed in our experiment occurs when the wire circuit is suddenly opened. Assuming that the capacitor was fully charged ($-V$) before the circuit was opened, the time evolution of the capacitor's voltage is expressed by

$$V_C(t) = -V\exp\left[-\frac{(t-t_o)}{\tau'}\right], \tag{12}$$

with the genuine relaxation time constant

$$\tau' = \frac{C}{1/R_C + 1/R_a} \tag{13}$$

and with t_0 being the moment when the electric conduction through the wire circuit was interrupted. If we consider that the voltage relaxation across the capacitor is due mainly to the effect of charge leakage by conduction through the dielectric material ($R_a \gg R_C$), then the following approximations are justified:

$$\tau \cong \tau_r = R_C C, \tag{14}$$

$$V_C(t) \cong -V\exp\left[-\frac{(t-t_o)}{\tau_r}\right], \tag{15}$$

where τ_r is the approximate relaxation time constant of the crystal.

Assuming that the conduction through the capacitor is predominantly of the ohmic type, we can relate the relaxation time constant τ_r to the bulk resistivity ρ_x and the dielectric constant ε_x in the x direction of the $BaTiO_3$ crystal by

$$\tau_r = \rho_s \varepsilon_x \varepsilon_0. \tag{16}$$

The permittivity of free space has the value[19] $\varepsilon_0 = 8.85 \times 10^{-12}\ \mathrm{C^2\,N^{-1}\,m^{-2}}$, and the dielectric constant of $BaTiO_3$ in the x direction (polar axis in z direction) is $\varepsilon_x = 3600$.[20,21]

B. Optical Model

In this second part of the theoretical treatment we will derive the optical intensity transients by integrating the electrical transients derived above with the quadratic electro-optic (Kerr) effect. The reason that the first-order electro-optic (Pockels) effect does not play any role in this experiment was explained in our previous paper.[1] A schematic of the intensity modulation process is shown in Fig. 1. Below are the consecutive physical steps through the optical system and their corresponding equations.

After exiting the 45° polarizer the amplitudes of the two orthogonal polarizations become equal and are given by

$$A_{y0} = A_{z0} = A_0. \tag{17}$$

After passing through the $BaTiO_3$ sample, the two transmitted amplitudes are

$$A_y = A_0 \exp(i\phi_y), \tag{18}$$

$$A_z = A_0 \exp(i\phi_z), \tag{19}$$

with

$$\phi_y = \frac{2\pi}{\lambda}(n_y - 1)l_x, \tag{20}$$

$$\phi_z = \frac{2\pi}{\lambda}(n_z - 1)l_x, \tag{21}$$

being the extra phases acquired after the transmission of light with wavelength λ through the bulk of the crystal and l_x is the length of the crystal in the direction of the normally incident light (x direction). The n_y and n_z are the indices of refraction corresponding to the y and z polarizations and are related to the electric field applied across the sample in the x direction (E_1) by the quadratic electro-optical formulas

$$\frac{1}{n_y^2} = \frac{1}{n_o^2} + R_{12}E_1^2, \tag{22}$$

$$\frac{1}{n_z^2} = \frac{1}{n_e^2} + R_{13}E_1^2. \tag{23}$$

Since the changes in the indices of refraction due to the Kerr effect are very small for $BaTiO_3$ ($\Delta n \approx 10^{-3}, 10^{-4}$),[22–25] it is convenient and appropriate to replace the two exact formulas above with two simpler, though approximate, formulas:

$$n_y \cong n_o - \frac{n_o^3}{2} R_{12}E_1^2, \tag{24}$$

$$n_z \cong n_e - \frac{n_e^3}{2} R_{13}E_1^2. \tag{25}$$

For $BaTiO_3$, which is a negative uniaxial crystal in the tetragonal state, $n_o = 2.413$ and $n_e = 2.361$ at $\lambda = 632.8$ nm.[26] The $R_{12} = -3.5 \pm 0.3 \times 10^{-17}$ m^2/V^2, and $R_{13} = -8.0 \pm 0.7 \times 10^{-17}$ m^2/V^2 are the Kerr electro-optic coefficients, which were experimentally determined in our previous paper, and they are labeled according to Nye's suffix abbreviation:[27] (11)→1; (22)→2; (33)→3; (23), (32)→4; (13), (31)→5; (12), (21)→6. In that paper,[1] in order to obtain the values for each of the two Kerr coefficients individually and with high precision, the phenomenon of electrostriction and the net effect of multiple reflections were taken into account in the set of equations describing the amplitude modulation; absorption was neglected.[28] In this paper we will derive the set of amplitude modulation equations by following the conventional approach throughout the optical modulation literature, which is to tacitly ignore all three of the phenomena mentioned above. This neglect is well justified here, because none of those three phenomena has any important effect on the general theoretical description of the behavior of the modulated relative intensities of light.

After passing through the Wollaston prism, which is rotated counterclockwise by $\theta = 15°$ in the plane normal to the incident direction of light, the orthogonally polarized amplitudes have the final form

$$A_y' = A_y \cos(\theta) - A_z \sin(\theta), \tag{26}$$

$$A_z' = A_y \sin(\theta) + A_z \cos(\theta). \tag{27}$$

By multiplying the above amplitudes with their complex conjugates, we obtain the following expressions for their corresponding modulated absolute intensities:

$$I_y' = I_0[1 - \sin(2\theta)\cos(\Delta\phi)], \tag{28}$$

$$I_z' = I_0[1 + \sin(2\theta)\cos(\Delta\phi)]. \tag{29}$$

Here

$$I_0 = A_0^2, \tag{30}$$

and

$$\Delta\phi = \frac{2\pi}{\lambda}(n_z - n_y)l_x \tag{31}$$

is the phase difference between the two orthogonal polarizations. For virgin crystal, this phase difference has the form

$$\Delta\phi_0 = \frac{2\pi}{\lambda}(n_e - n_o)l_{x0}, \tag{32}$$

and the corresponding modulated absolute intensities are

$$I_{y0}' = I_0[1 - \sin(2\theta)\cos(\Delta\phi_0)], \tag{33}$$

$$I_{z0}' = I_0[1 + \sin(2\theta)\cos(\Delta\phi_0)], \tag{34}$$

where $l_{x0} = 1$ mm and has been provided by the manufacturer.[29] The relation between l_x and l_{x0} is given by

$$l_x = l_{x0}(1 + s_x), \tag{35}$$

where $s_x = 0.10 \pm 0.05\%$ is the electrostrictive strain for an unclamped, (100) single crystal of $BaTiO_3$, subject to electric fields between 1×10^5 V/m and 7×10^5 V/m. The value of the electrostrictive strain was obtained from a previous graph of strain versus electric field (at no external stress) obtained by Burcsu and co-workers[30,31] for the same type of $BaTiO_3$ crystal as ours, having the same specifications and even purchased from the same company.[29] The phenomenon of electrostriction is neglected in this paper, so

$$l_x \cong l_{x0}. \tag{36}$$

Taking this approximation into consideration, the electric field across the sample as a function of time will be considered to be

$$E_1(t) = \frac{V_C(t)}{l_{x0}}. \tag{37}$$

For $V_C(t)$ we will use the expressions given by Eqs. (9), (11), and (15) throughout this paper.

Finally, we get the equations for the modulated relative intensities:

$$I_{yr}{}' = \frac{I_y{}'}{I_{y0}{}'} = \frac{1 - \sin(2\theta)\cos(\Delta\phi)}{1 - \sin(2\theta)\cos(\Delta\phi_0)}, \tag{38}$$

$$I_{zr}{}' = \frac{I_z{}'}{I_{z0}{}'} = \frac{1 + \sin(2\theta)\cos(\Delta\phi)}{1 + \sin(2\theta)\cos(\Delta\phi_0)}. \tag{39}$$

It is this set of equations that we will use to model the time evolution of our modulated intensities for the three types of transient behavior described in Section 1. By curve-fitting these equations with the optical experimental data presented in Figs. 2 and 3, we will be able to extract the value of the excitation time constant τ_e associated with the first type of transient, the switching time constant τ_s, associated with the second type, and the value of the relaxation time constant τ_r corresponding to the third type of transient. From τ_r we will be able to deduce the electrical resistivity ρ_x (at room temperature) of the bulk $BaTiO_3$ sample by using Eq. (16).

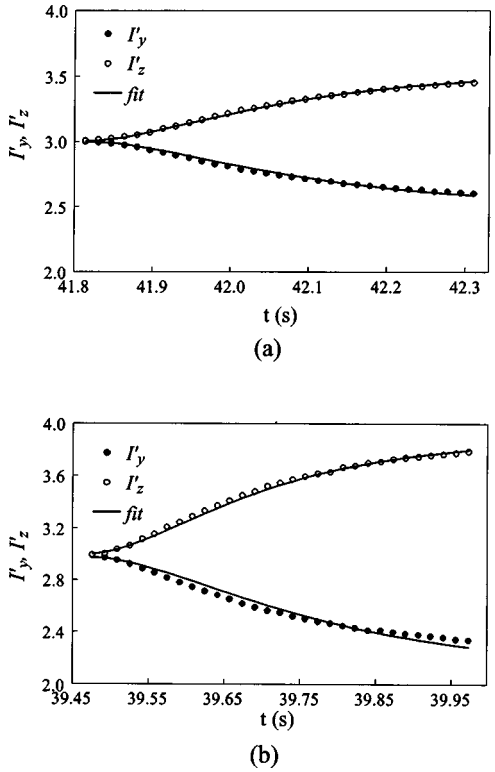

Fig. 6. Plot of the curve-fitted intensities corresponding to the excitation transients when the applied electric field had just been changed from (a) 0 V/mm to +400 V/mm during the first experimental trial and (b) 0 V/mm to −400 V/mm during the second experimental trial. The interval between the plotted graph values is of ten data points for each case.

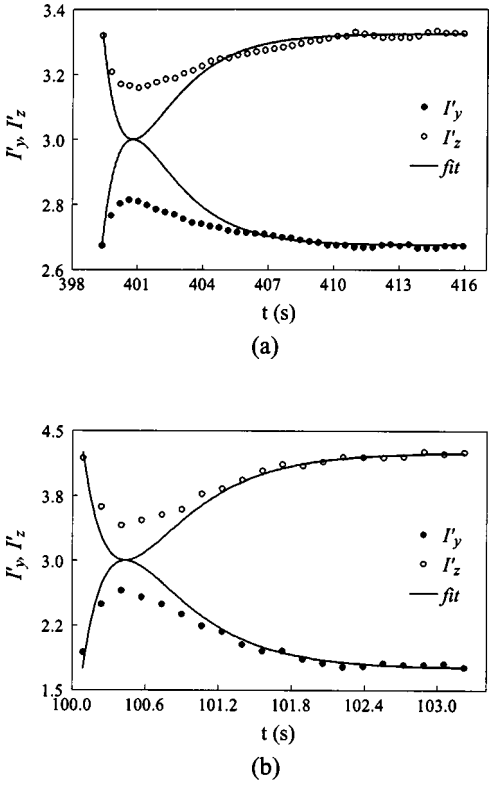

Fig. 7. Plot of the curve-fitted intensities corresponding to the switching transients when the applied electric field had just been changed from (a) +200 V/mm to −200 V/mm during the first experimental trial, (b) −400 V/mm to +400 V/mm during the second experimental trial. The interval between the plotted graph values is of twenty data points for the first experimental trial and ten data points for the second experimental trial. The gap between the extreme values of the experimental data curves and those of the corresponding fitted curves is due to dielectric absorption, a form of switching inertia common to all bulk crystal dielectrics.

4. DISCUSSION

In Figs. 6–9 we show the intensity-versus-time experimental and fitted curves corresponding to the transition regimes generated at the moment time when the applied electric field changes to new values. The curve fitting was done with PSI-Plot (Version 7). The extracted time constants for the excitation (τ_e), switching (τ_s), and relaxation (τ_r) corresponding to the time transient processes in the light intensities, and indirectly in the refractive indices, are posted in Tables 1 and 2 for different applied electric fields. By using Eq. (16), we were able to deduce the electrical resistivity of our piece of bulk single crystal $BaTiO_3$, which is also dependent on the electric field across the sample as shown in our table. According to Eq. (16), the variation of ρ_x with E_1 is mainly a consequence of the actual nonlinear dependence of ε_x with E_1; this is a basic characteristic of ferroelectrics. Also, considering that we are dealing with a nonlinear dielectric, it is very probable that the electrical resistivity, like most of the other physical parameters, might in itself have a certain dependence on the externally applied electrical stress. Our deduced values for the room-temperature resistivity of single-crystal tetragonal $BaTiO_3$ are almost five times the values determined by Boyeaux and

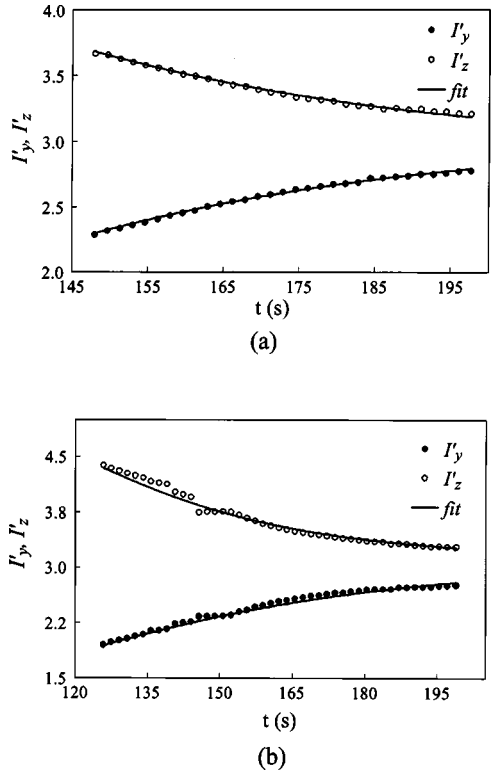

Fig. 8. Plot of the curve-fitted intensities corresponding to the relaxation transients when the electric circuit was opened after having the $BaTiO_3$ crystal under a constant (a) −400 V/mm during the first experimental trial and (b) +400 V/mm during the second experimental trial. The interval between the plotted graph values is of ten data points for each case.

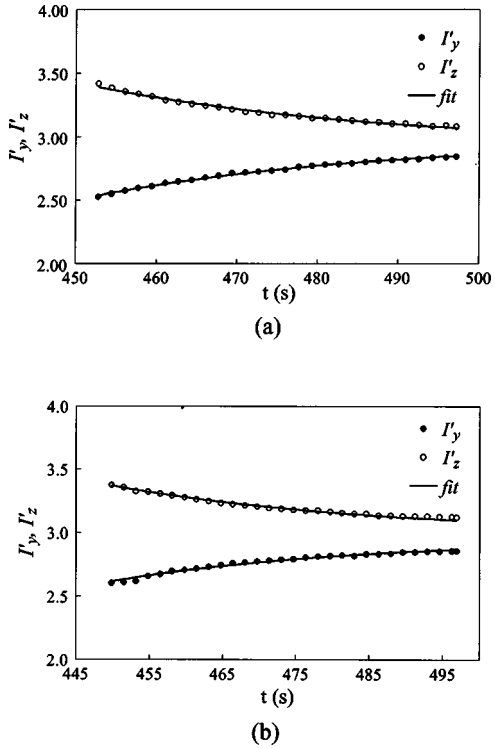

Fig. 9. Same as Fig. 8 but for a constant (a) −200 V/mm during the first experimental trial and (b) +200 V/mm during the second experimental trial. The interval between the plotted graph values is often data points for each case.

Michael-Calendini[32] and by Gilbert *et al.*,[33] who used an electrical method based on the measurement of the drift mobility of the charge carriers. There could be many reasons for the discrepancy between their values and ours, the main one of which is that the resistivity of ferroelectrics depends very sensitively on the number and type of impurities in the crystal; unfortunately, the stoichiometry of our crystals was not provided by the seller. Another reason might merely be that Eq. (16) is a formula that properly applies only to linear dielectrics; for nonlinear dielectrics, this formula should provide a good approximation only at very low electric fields. A last reason could be the appearance in bulk single crystal ferroelectrics of space charge regions and surface charge layers that alter the charge conduction processes in these materials.[14–17,34–36]

The two intensity-versus-time graphs also reveal two new and interesting phenomena, which we will qualitatively describe and explain. One phenomenon is the discrepancy between the intensity values of light, for both polarizations, when the applied electric field is inverted from +600 V/mm to −600 V/mm and vice versa. The other is the abrupt, steplike change in the light intensity for the two polarizations at a point during the relaxation phase of the crystal.

Table 1. Magnitudes of the Time Constants for the Three Types of Transients and the Deduced Values of the Bulk Electrical Conductivity of Tetragonal $BaTiO_3$: Experimental Trial 1

E_1 (V/mm)	τ (s)	ρ (10^9 Ωm)
Excitation		NA
process	τ_e	
0 to +400	0.25±0.02	
Switching		
process	τ_s	
+200 to −200	1.3±0.4	
Relaxation		
process	τ_r	ρ_x (10^9 Ωm)
−400 to 0	72±5	2.2±0.2
−200 to 0	59±5	1.8±0.2

Table 2. Magnitudes of the Time Constants for the Three Types of Transients and the Deduced Values of the Bulk Electrical Conductivity of Tetragonal $BaTiO_3$: Experimental Trial 2

E_1 (V/mm)	τ (s)	ρ (10^9 Ωm)
Excitation		NA
process	τ_e	
0 to −400	0.20±0.05	
Switching		
Process	τ_s	
−400 to +400	0.6±0.1	
Relaxation		
process	τ_r	ρ_x (10^9 Ωm)
+400 to 0	68±5	2.1±0.2
+200 to 0	56±2	1.7±0.2

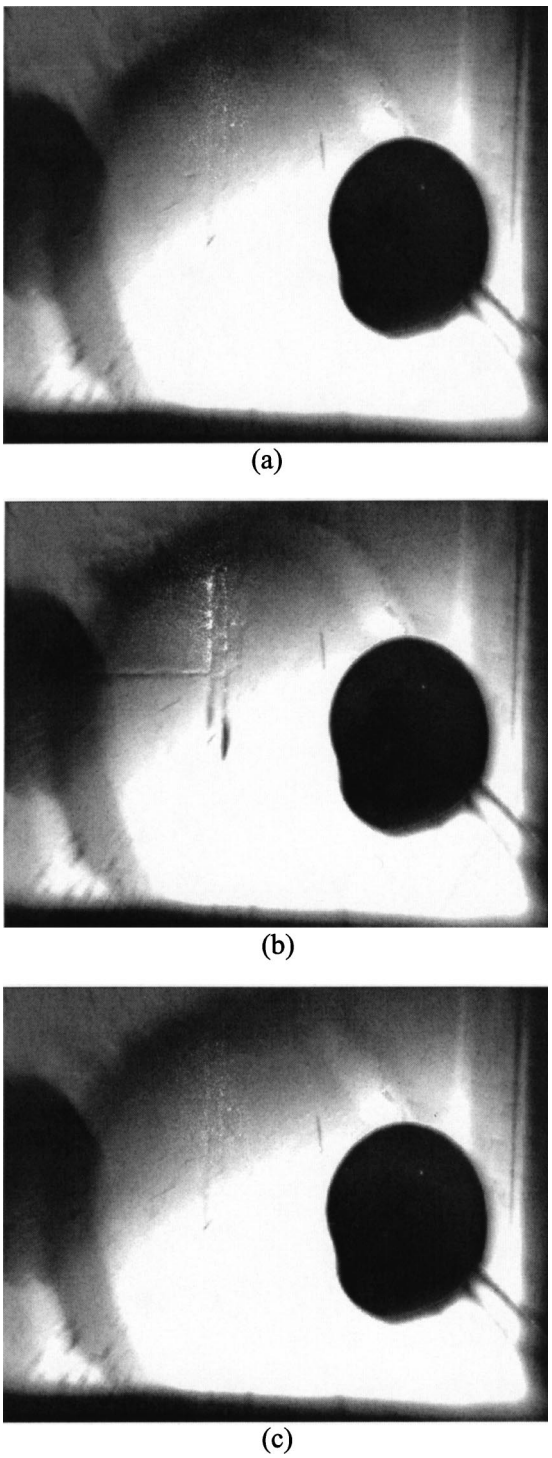

Fig. 10. Pictures of $BaTiO_3$ crystal's surface taken with the CCD camera during the first experimental trial; presented in chronological order are the crystal's images at (a) +600 V/mm, (b) −600 V/mm, and (c) the first few seconds after the electrical circuit was opened.

Some striking changes at the surface of the sample due to polysynthetic twinning[37] were detected by the CCD camera when the voltage was inverted from plus to minus 600 V/mm (see Figs. 10 and 11). These variations in the surface morphology of the crystal led to a more diffuse light transmission, especially for the light polarized in the z' direction; this was confirmed by the pictures of the light's spatial distribution on the screen taken with the digital camera (S and DC, respectively, in Fig. 4) (see Figs. 12 and 13). The diffuse scattering had the negative effect of reducing the amount of light entering the two detectors, thus decreasing the measured values of the light intensity. We suspect that the reason for the twinning at −600 V/mm and not at +600 V/mm is that our $BaTiO_3$ crystal had accumulated some bias residual polarization

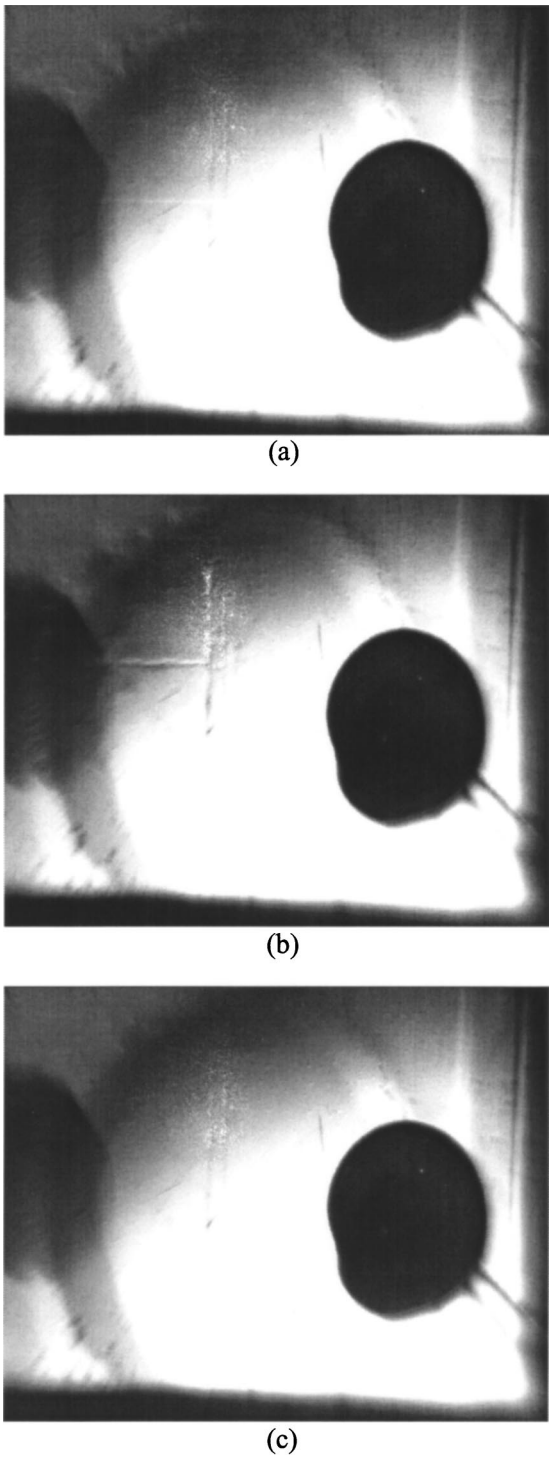

Fig. 11. Same as Fig. 10 but for the second experimental trial with images at (a) +600 V/mm, (b) −600 V/mm, and (c) the first few seconds after the electrical circuit was opened.

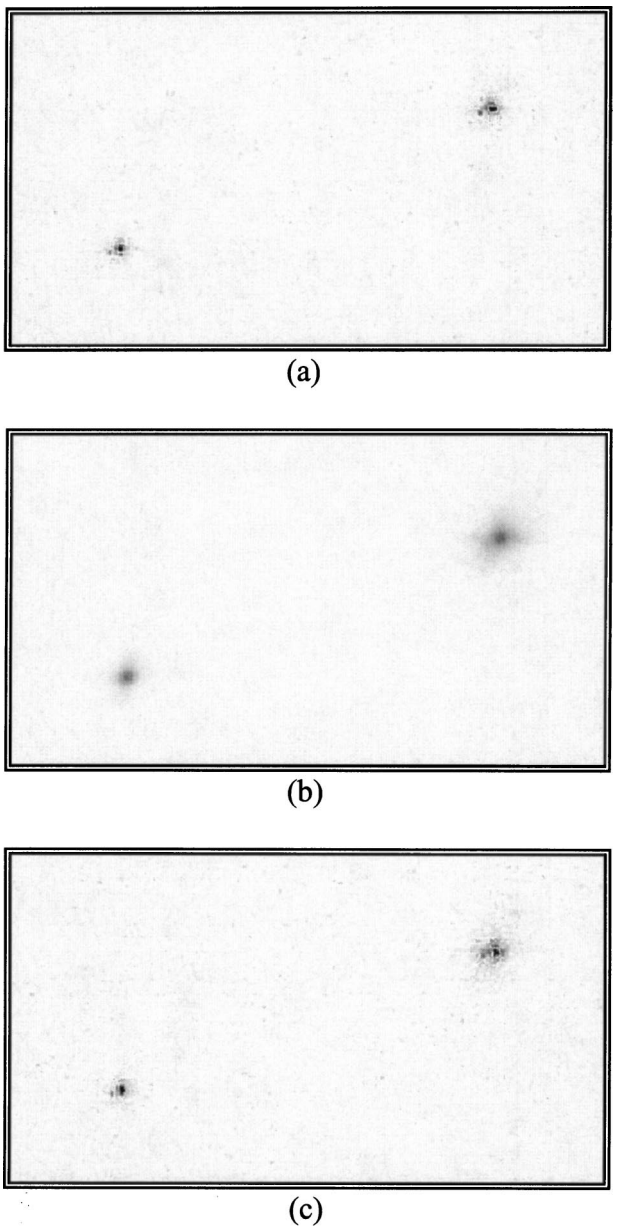

Fig. 12. Images (in negative) of the two polarized light distributions on the screen taken with the digital camera during the first experimental trial. Presented in chronological order are the pair of light spots at (a) +600 V/mm, (b) −600 V/mm, and (c) the first few seconds after the electrical circuit was opened.

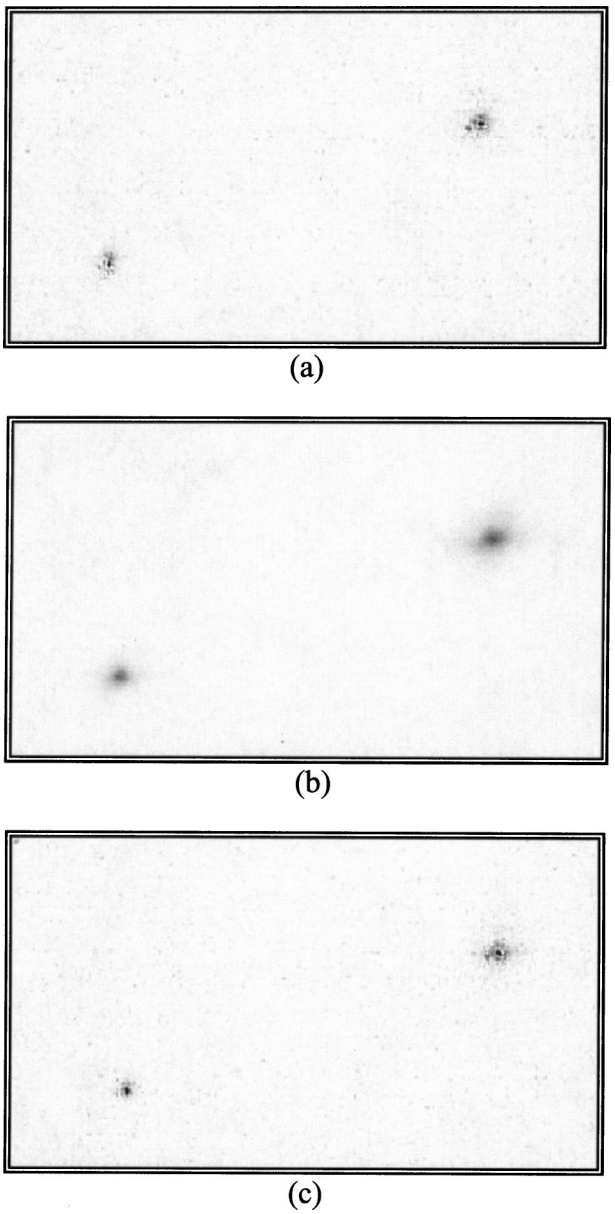

Fig. 13. Same as Fig. 12 but for the second experimental trial with the pair of light spots at (a) +600 V/mm, (b) −600 V/mm, (c) first few seconds after the electrical circuit was opened.

in the negative direction of the electric field. This twinning phenomenon could also provide a qualitative explanation for the odd behavior of the light intensity when the electric circuit is suddenly opened after the sample has been kept under a −600 V electrical potential for some time. As soon as the applied −600 V potential is canceled by the opening of the electric circuit, two phenomena occur simultaneously. The first one corresponds to the elastic property[38,39] of the crystal's surface morphology to return to its initial shape once the electrical stress has been removed. This causes the short-term behavior of the transmitted light intensity, which acts as if the $BaTiO_3$ sample were under a +600-V/mm applied electric field. The second phenomenon is caused by the relaxation of the

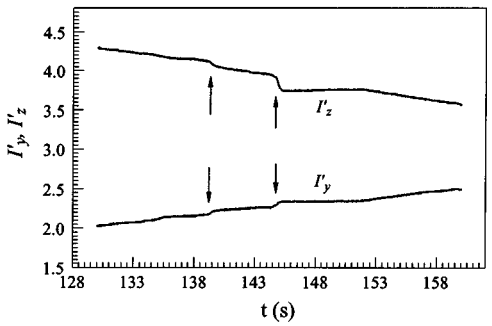

Fig. 14. Magnified picture of the discontinuous intensity regions in Fig. 8(b). This steplike behavior in the intensity patterns is considered by the authors to be an optical analog of the ferroelectric Barkhausen effect.

indices of refraction back to their original values; in this paper, this has already been classified as a third type of transient. Eventually, the latter phenomenon begins to dominate the former, and after awhile the two intensities start to relax back to their original values corresponding to the initially undisturbed ferroelectric crystal; this trend in the two polarized intensities was better captured during the second experimental trial.

In Fig. 14 we show a magnified picture of the jumplike changes in the two polarized intensities a period of time after the electric circuit is opened. The monitoring intensity during that period of time indicates that those polarized intensity variations are not caused by some temporary alteration in the incident intensity of the laser. Furthermore, the fact that the I_z' intensity decreases while simultaneously the I_y' intensity increases is a clear indication that the steplike changes in these intensities are not related to some unexpected absorption in the sample; absorption would have caused both intensities to decrease at the same time. The only cause for these intensity jumps is the sudden change in the real part of the refractive indices of $BaTiO_3$ during this time. By analyzing this time variation of the optical indices, one might be able to extract some information about the domain kinematics in the ferroelectric crystal. Because of the jumplike time evolution of the above effect, we are inclined to classify this phenomenon as the optical analog of the ferroelectric Barkhausen effect.[40–47]

5. CONCLUSION

When subjected to an externally applied electric voltage, a ferroelectric sample of bulk $BaTiO_3$ changes its indices of refraction as a result of the electro-optic effect. When probed with laser light, these changes in the refractive indices cause variations in the transmitted intensities of light beams that are polarized in the directions corresponding to each of the indices. When the electric field across the crystal abruptly changes in either value or direction, the intensity of the transmitted light behaves in ways that we labeled as optical transients, by analogy with the electrical transients known in electrical circuit literature. By modeling and analyzing the intensity of light in the transient regimes, we were able to obtain some quantitative information regarding the time constants of these optical transients in the particular case of a (100) $BaTiO_3$ single crystal at room temperature. In one case, however, we detected some interesting steplike changes in the light intensities during the crystal's relaxation process; for lack of any previous evidence in the scientific literature, we ventured to consider them some form of optical analog of the known ferroelectric Barkhausen effect. We also deduced some values for the electrical resistivity of our $BaTiO_3$ bulk sample for different applied voltages; these were calculated by using only optical data as experimental input. Although our values for resistivity proved to be approximately five times larger than values previously measured by Boyeaux and Michael-Calendini[32] and by Gilbert *et al.*,[33] who used an electrical method, we feel confident that if our sample had been characterized by the same physical parameters (stoichiometry, thickness) as theirs, then the discrepancy between their values and ours would have been much smaller.

We have shown previously[1] that our optical method can be applied successfully not only to $BaTiO_3$ but also to 18 out of 20 noncentrosymmetric crystal classes in which both first-order (Pockels) and second-order (Kerr) electro-optic effects coexist; this gives it a very wide area of application in crystal optics. The generality of this method can make it very useful in the fields of solid-state physics where the dynamics of symmetry transitions in crystals is a subject of research, because it can supplement the ongoing theoretical effort with an *in situ* experimental method.

ACKNOWLEDGMENTS

The authors acknowledge support from the Texas Higher Education Coordinating Board Advanced Research Program. We also thank C. L. Chen and X. H. Chen for depositing the gold electrodes on the sample.

Corresponding author L. T. Wood's e-mail address is ltwood@uh.edu.

REFERENCES

1. M. Melnichuk and L. T. Wood, "Method for measuring off-diagonal Kerr coefficients by using polarized light transmission," J. Opt. Soc. Am. A **22**, 377–384 (2005).
2. F.-S. Chen, "Modulators for optical communications," Proc. IEEE **58**, 1440–1457 (1970).
3. A. R. Johnston and J. M. Weingart, "Determination of the low-frequency linear electro-optic effect in tetragonal $BaTiO_3$," J. Opt. Soc. Am. **55**, 828–834 (1965).
4. I. P. Kaminow, *An Introduction to Electrooptic Devices* (Academic, New York, 1974).
5. C. C. Davis, *Lasers and Electro-Optics* (Cambridge U. Press, Cambridge, UK, 1996).
6. A. Yariv and P. Yeh, *Optical Waves in Crystals* (Wiley, Hoboken, N.J., 2003).
7. A. Yariv, *Optical Electronics in Modern Communications* (Oxford U. Press, New York, 1997).
8. R. D. Guenther, *Modern Optics* (Wiley, Hoboken, N.J., 1990).
9. B. E. A. Saleh and M. C. Teich, *Fundamentals of Photonics* (Wiley, Hoboken, N.J., 1991).
10. K. Iizuka, *Elements of Photonics* (Wiley, Hoboken, N.J., 2002).
11. E. Hecht, *Optics*, 4th ed. (Pearson Addison-Wesley, Boston, Mass., 2001).
12. M. V. Klein and T. E. Furtak, *Optics*, 2nd ed. (Wiley, Hoboken, N.J., 1986).
13. G. Fowles, *Introduction to Modern Optics*, 2nd ed. (Dover, New York, 1989).
14. F. Jona and G. Shirane, *Ferroelectric Crystals* (Pergamon, New York, 1962). (Reprint, Dover, New York, 1993).
15. J. C. Burfoot, *Ferroelectrics—An Introduction to the Physical Principles* (Van Nostrand, London, 1967).
16. M. E. Lines and A. M. Glass, *Principles and Applications of Ferroelectrics and Related Materials* (Clarendon, Oxford, UK, 1977).
17. J. C. Burfoot and G. W. Taylor, *Polar Dielectrics and Their Applications* (MacMillan, London, 1979).
18. L. O. Chua, C. A. Desoer, and E. S. Kuh, *Linear and Nonlinear Circuits* (McGraw-Hill, New York, 1987).
19. D. J. Griffiths, *Introduction to Electrodynamics*, 3rd ed. (Prentice Hall, Englewood Cliffs, N.J., 1999).
20. M. J. Weber, *Handbook of Optical Materials* (CRC Press, Boca Raton, Fla., 2003).

21. R. L. Sutherland, *Handbook of Nonlinear Optics*, 2nd ed. (Marcel Dekker, New York, 2003).
22. D. Mayerhofer, "Transition to the ferroelectric state in barium titanate," Phys. Rev. **112**, 413–423 (1958).
23. W. Haas, R. Johannes, and P. Cholet, "Light beam deflection using the Kerr effect in single crystal prisms of $BaTiO_3$," Appl. Opt. **3**, 988–989 (1964).
24. V. É. Perfilova and A. S. Sonin, "The electrooptic properties of single crystals of barium titanate," Sov. Phys. Solid State **8**, 82–84 (1966).
25. A. S. Sonin and V. É. Perfilova, "Electrooptical properties of barium titanate in the paraelectric phase," Sov. Phys. Crystallogr. **14**, 419–420 (1969).
26. K. H. Hellwege, *Landolt-Börnstein*, *New Series* III/2 (Springer-Verlag, Berlin, 1969).
27. J. F. Nye, *Physical Properties of Crystals* (Oxford U. Press, New York, 2001).
28. M. E. Drougard and D. R. Young, "Domain clamping effect in barium titanate single crystals," Phys. Rev. **94**, 1561–1564 (1954).
29. M. T. I. Corporation, www.mticrystal.com.
30. E. Burcsu, G. Ravichandran, and K. Bhattacharya, "Electro-mechanical behaviour of 90-degree domain motion in barium titanate single crystals," in *Smart Structures and Materials 2001: Active Materials: Behavior and Mechanics*, C. S. Lynch, ed., Proc. SPIE 4333, 121–130 (2001).
31. E. Burcsu, "Investigations of large strain actuation in barium titanate," Ph.D. thesis (California Institute of Technology, Pasadena, Calif., 2001), http://etd.caltech.edu/etd/available/etd-10232001-192042/.
32. J. P. Boyeaux and F. M. Michael-Calendini, "Small polaron interpretation of $BaTiO_3$ transport properties from drift mobility measurements," J. Phys. C **12**, 545–556 (1979).
33. S. R. Gilbert, L. A. Wills, B. W. Wessels, J. L. Schindler, J. A. Thomas, and C. R. Kanewurf, "Electrical transport properties of epitaxial $BaTiO_3$ thin films," J. Appl. Phys. **80**, 969–977 (1996).
34. W. Känzig, "Space charge layer near the surface of a ferroelectric," Phys. Rev. **98**, 549–550 (1955).
35. S. Triebwasser, "Space charge fields in $BaTiO_3$," Phys. Rev. **118**, 100–105 (1960).
36. A. Branwood, O. H. Hughes, J. D. Hurd, and R. H. Tredgold, "Evidence for space charge conduction in barium titanate single crystals," Proc. Phys. Soc. London **79**, 1161–1165 (1962).
37. M. V. Klassen-Neklyudova, *Mechanical Twinning of Crystals* (Kluwer-Consultants Bureau, Norwell, Mass., 1964).
38. E. K. H. Salje, *Phase Transitions in Ferroelastic and Coelastic Crystals* (Cambridge U. Press, Cambridge, UK, 1990).
39. V. S. Boyko, R. I. Garber, and A. M. Kossevich, *Reversible Crystal Plasticity* (AIP Press, New York, 1994).
40. R. R. Newton, A. J. Ahearn, and K. G. McKay, "Observation of the ferro-electric Barkhausen effect in barium titanate," Phys. Rev. **75**, 103–106 (1949).
41. A. G. Chynoweth, "Barkhausen pulses in barium titanate," Phys. Rev. **110**, 1316–1332 (1958).
42. R. C. Miller, "Some experiments on the motion of 180° domain walls in $BaTiO_3$," Phys. Rev. **111**, 736–739 (1958).
43. A. G. Chynoweth, "Effect of space charge fields on polarization reversal and the generation of Barkhausen pulses in barium titanate," J. Appl. Phys. **30**, 280–285 (1959).
44. V. M. Rudyak, "The Barkhausen effect," Sov. Phys. Usp. **13**, 461–479 (1971).
45. V. M. Rudyak, A. Yu. Kudzin, and T. V. Panchenko, "Barkhausen jumps and stabilization of the spontaneous polarization of single crystals of $BaTiO_3$," Sov. Phys. Solid State **14**, 2112–2113 (1973).
46. S. A. Flerova, Yu. I. Samchenko, and V. M. Gorbenko, "Light emission during pulsed repolarization of deformed $BaTiO_3$ crystals," Sov. Phys. Solid State **23**, 1624–1625 (1981).
47. V. V. Belov and O. Yu. Serdobol'skaya, "Emission of sound associated with polarization reversal in a ferroelectric crystal," Sov. Phys. Solid State **26**, 868–870 (1984).

Curriculum Vitae

Mike Melnichuk

University of Wisconsin-Milwaukee (UWM), Rm. 411
(E-mail): mike_melnichuk@sbcglobal.net (preferably) or melnickm@uwm.edu
(Phone): (414)-362-0071 (preferably) or (414)-229-6708
(Fax): (414)-229-5589 (Attn. Dr. Mike Melnichuk)

Education

B.S. in Physics & Minor in Mathematics (August, 1995) University of Houston (UH)
Ph.D. in Physics (December, 2004) (UH)
Postdoctoral Research Associate in Biophotonics (Present) (UWM)

Professional and Honorary Societies

American Physical Society

Chronology of Experience

February 1996 – August 1997, Production Engineer/Supervisor, Daily Instruments Corp.
Fall Semester 1997, Post-baccalaureate, Physics (UH)
Spring 1998 – Fall 1999, Teaching Assistant, Physics (UH)
Spring 2000 – Spring 2001, Research Assistant, Physics (UH)
Fall 2001 – Spring 2002, (50%) Teaching and (50%) Research Assistant, Physics (UH)
Fall 2002 – Fall 2004, Teaching Assistant, Physics (UH)
January 2005 – May 2005, Administrator/Supervisor, Physics Learning Center (UH)
June 2005 – Present, Postdoctoral Research Associate in Biophotonics (UWM)

Journal Article Publications

1. "Fraunhofer diffraction to determine the twin angle in single crystal $BaTiO_3$," Mike Melnichuk and Lowell T. Wood, Appl. Opt. **42**, 4463-4467 (2003).
2. "Method for measuring off-diagonal Kerr coefficients by using polarized light transmission," Mike Melnichuk and Lowell T. Wood, J. Opt. Soc. Am. A **22**, 377-384 (2005).
3. "Time-resolved optical transients in tetragonal $BaTiO_3$," Mike Melnichuk and Lowell T. Wood, J. Opt. Soc. Am. A **22**, 734-744 (2005).
4. "Determining selected quadratic coefficients in noncentrosymmetric crystals," Mike Melnichuk and Lowell T. Wood, J. Opt. Soc. Am. A **23**, No. 5, *7 journal pages; page numbers-not provided yet*, May (2006).

Contributed Talks (Abstracts)

"Determination of the Twin Angle in Single Crystal $BaTiO_3$ Using Fraunhofer Diffraction" Mike Melnichuk and Lowell T. Wood (Paper presented at the American Physical Society Meeting, Austin, TX, March 2003).

Fields of Research Interest

Biophysics, Optics, Condensed Matter – experimental and/or theoretical.

Fraunhofer diffraction to determine the twin angle in single-crystal $BaTiO_3$

Mike Melnichuk and Lowell T. Wood

We present a new method for determining the electrically induced twin angle α of a (100) bulk single crystal of barium titanate ($BaTiO_3$) using a nondestructive optical technique based on Fraunhofer diffraction. The technique required two steps that were performed simultaneously. First, we analyzed the diffracted light intensity captured with a line camera. Second, we measured the size of the diffracting element by analyzing images of the crystal's surface taken with a CCD camera. The value obtained for the twin angle is $0.67° \pm 0.05°$, which compares favorably with the theoretical value of 0.63°.

OCIS codes: 050.0050, 160.0160, 120.0120, 050.1960, 120.5820, 160.2260.

1. Introduction

When an electric field is applied along the z direction of a (100) tetragonal sample of a barium titanate ($BaTiO_3$) bulk crystal, 90°-type ferroelectric domains (polysynthetic twins[1]) start to appear. The presence of these twins causes a detectable change in the surface morphology of the crystal at the 90° domain boundaries as can be seen in Fig. 1(a). The angle between the polar axes of two adjacent domains is equal to $90° - \alpha$, where α is the twin angle and is given by

$$\tan\left(\frac{90° - \alpha}{2}\right) = \frac{a}{c}. \tag{1}$$

See Fig. 1(b).

For barium titanate in the tetragonal phase, the unit cell values $a = 3.992$ Å and $c = 4.036$ Å give the ratio $a/c \cong 0.989$.[2] Use of Eq. (1) leads to a theoretical value of 0.63° for α. The magnitude determination of the twin angle of several perovskites has been done before, and to our knowledge, in all previous experiments at least one of the following four major microscopy techniques was used: atomic force microscopy,[3–8] kelvin force microscopy,[7] scanning force microscopy,[9,10] or piezoelectric (piezoresponse) force microscopy.[10,11]

In this paper we present a new technique for determining the angle α using light scattering instead of microscopy. Here the twin angle is deduced from the intensity distribution of laser light scattered from one of the morphologically deformed faces of a tetragonal (100) single crystal of $BaTiO_3$ when a strong electric field of 600 V/mm is applied across the sample in the z direction.

2. Theory

To understand laser-light scattering from the sample, the electrically induced surface shape of a $BaTiO_3$ sample can be modeled as a quasi-periodic diffraction grating with the diffraction element having the form shown in Fig. 2. The normalized intensity distribution I as a function of the scattered angle θ for this type of grating having N periodic elements can be written as

$$I(\theta) = I_n F(\theta) S(\theta), \tag{2}$$

where

$$F(\theta) = A^2\{\mathrm{sinc}[\Phi_A(\theta)]\}^2 + C^2\{\mathrm{sinc}[\Phi_C(\theta)]\}^2 + 2AC\cos[\Phi(\theta)], \tag{3}$$

$$S(\theta) = \left\{\frac{\sin[N\Phi(\theta)]}{N\sin[\Phi(\theta)]}\right\}^2, \tag{4}$$

$$\Phi(\theta) = \Phi_A(\theta) + \Phi_C(\theta), \tag{5}$$

$$\Phi_A(\theta) = \frac{\pi A}{\lambda}[\sin(\theta) - \sin(\theta_0)], \tag{6}$$

$$\Phi_C(\theta) = \frac{\pi C}{\lambda\cos(\alpha)}[\sin(\theta - \alpha) - \sin(\theta_0 + \alpha)]. \tag{7}$$

The authors are with the Department of Physics, University of Houston, 617 Science and Research Building One, Houston, Texas 77204-5005. L. T. Wood's e-mail address is ltwood@uh.edu.

Received 19 December 2002; revised manuscript received 17 April 2003.

0003-6935/03/224463-05$15.00/0

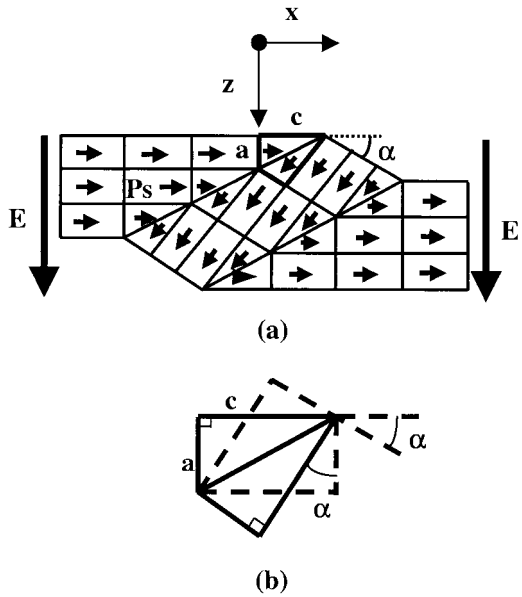

Fig. 1. Illustration of the electrically induced twin angle α in a (100) single crystal of $BaTiO_3$ when the electric field E is applied in the z direction. (a) A greatly exaggerated schematic in the x–z plane of the lattice matching at the 90° domain boundaries. (b) A magnified view of the twinned tetragonal unit cell; the tetragonality is also greatly exaggerated.

Here, I_n is the intensity normalizing factor; $F(\theta)$ is the intensity form factor; $S(\theta)$ is the intensity structure factor; $\Phi(\theta)$ is one half of the total phase difference between two adjacent diffraction elements; $\Phi_A(\theta)$ and $\Phi_C(\theta)$ are the phase differences generated by the A and C regions of the diffraction element, respectively; θ_0 is the specular reflection angle; λ is the laser wavelength; and α is the twin angle.

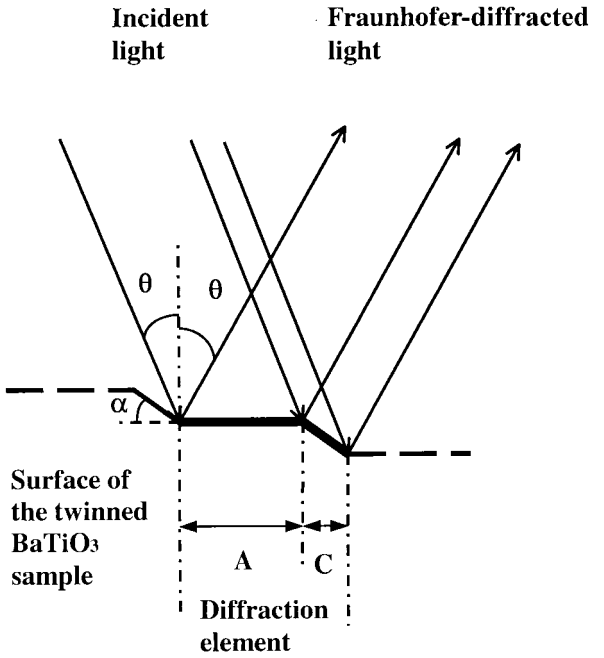

Fig. 2. Schematic of the theoretical model for the diffraction grating formed by the twinned surface of the $BaTiO_3$ sample.

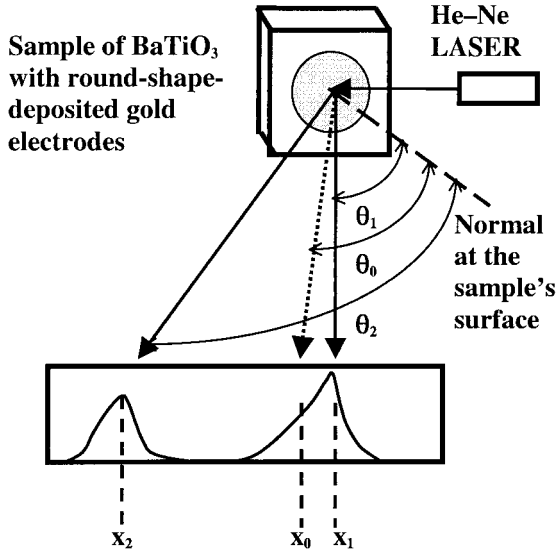

Fig. 3. Sketch illustrating the relationship between the position x of the diffraction maxima on the detector screen and the corresponding angle θ of the scattered beam. θ_0 and x_0 stand for the angle and the position, respectively, of the specularly reflected beam.

Because the angle θ cannot be measured directly, a more appropriate variable for the intensity function [Eq. (2)] would be the position x on the detector's screen. Figure 3 shows that this new variable (x) is related to the old variable (θ) by the expression

$$\tan(\theta_0 - \theta) = \frac{x - x_0}{R} = \frac{\Delta x}{R}, \tag{8}$$

where x_0 is the position of the specularly reflected beam when an electric field $E = 0$ V/mm was applied to the sample, and R is the distance between the detector and the sample.

In determining the angle α, we made use of the following three equations:

$$\tan(\theta_0 - \theta_1) = \frac{\Delta x_1}{R}, \tag{9}$$

$$\tan(\theta_0 - \theta_2) = \frac{\Delta x_2}{R}, \tag{10}$$

$$\Phi(\theta_2) - \Phi(\theta_1) = \pi, \tag{11}$$

where x_0, x_1, x_2, θ_1, and θ_2 are defined in Fig. 3.

Equations (9) and (10) relate the absolute values of the distances between the intensity peak of the specular beam ($E = 0$ V/mm) and the two principal adjacent maxima of the diffracted light ($E = 600$ V/mm). Equation (11) is derived by consecutively applying the condition for diffraction maxima to the zeroth- and first-order intensity peaks and then subtracting one from the other. By simultaneously solving Eqs. (9)–(11) we obtain an exact expression for the twin angle α given by

$$\tan(\alpha) = \frac{(A + C)\left\{\dfrac{R\,\sin(\theta_0) - (\Delta x_2)\cos(\theta_0)}{[R^2 + (\Delta x_2)^2]^{1/2}} - \dfrac{R\,\sin(\theta_0) - (\Delta x_1)\cos(\theta_0)}{[R^2 + (\Delta x_1)^2]^{1/2}}\right\} - \lambda}{C\left\{\dfrac{R\,\cos(\theta_0) + (\Delta x_2)\sin(\theta_0)}{[R^2 + (\Delta x_2)^2]^{1/2}} - \dfrac{R\,\cos(\theta_0) + (\Delta x_1)\sin(\theta_0)}{[R^2 + (\Delta x_1)^2]^{1/2}}\right\}}. \quad (12)$$

3. Experiment

The optical technique used in this experiment is based on the general idea that a laser beam scattering off a crystal reveals quantitative information about the sample's surface morphology without damaging it, and, in this way, the technique resembles one used previously by Klemradt *et al.*[12] The configuration of the experiment is shown schematically in Fig. 4.

The sample used was a 5 mm × 5 mm × 1 mm, one-face-polished, (100)-oriented, single crystal of barium titanate ($BaTiO_3$). For calibration purposes, a small ruler with a 0.5-mm resolution scale was glued to the base of the sample facing the CCD camera. Two gold electrodes, having a 200-Å thickness and a 3-mm diameter, were deposited by sputtering onto the 5 mm × 5 mm surfaces of the sample. A pair of thin gold wires was permanently attached to these electrodes by colloidal silver paste. The loose ends of the gold wires were connected to a high-voltage power supply. The polished side of the crystal was illuminated simultaneously by two sources of light. One source was an incandescent lamp that illuminated the surface of the sample to make it visible to the CCD camera (BASLER A101p, 1300 horizontal × 1030 vertical pixels, pixel size 6.7 μm × 6.7 μm), which provided a clear, real-time image of the sample's face. The other light source was a 0.5-mW He–Ne laser (wavelength of 632.8 nm) with a beam diameter of 0.48 mm at the $1/e^2$ points. After undergoing diffraction from the sample, the light was collected by a line camera detector (Thorlabs Model LC1, 3000 pixels, 7-μm pitch). This low-power laser was used because the intensity was sufficient for the diffraction measurements, and it did not produce changes in the sample temperature. All measurements were taken at a temperature of 23.5 °C.

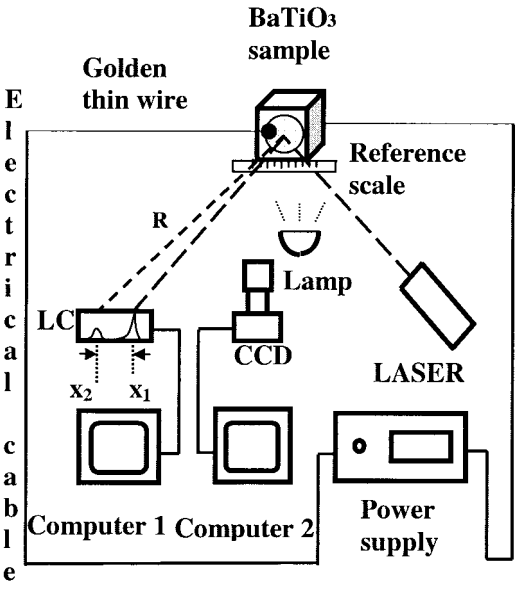

Fig. 4. Schematic of the experimental setup. LC, line camera.

Data were collected in the following way. The line camera's output of the diffracted intensity distribution and the CCD camera's image of the sample's surface were simultaneously monitored in real time on two computer screens, while the voltage across the sample was manually varied. When the diffracted intensity pattern changed, the image of the crystal's surface and the corresponding intensity distribution were recorded, along with the value of the applied voltage. The voltage was changed in steps of 100 V from 0 V to 600 V to 0 V to −600 V and back to 0 V. This process was repeated three times. Normally, the electrically induced twins form randomly across the sample's surface. To avoid having to use a statistical averaging process over the domain sizes, we selected a region where only two twins having almost identical widths (to four-digit precision according to the image analysis software) were illuminated by the laser beam. The modeling can then be easily carried out by setting $N = 2$ in Eq. (4). For the general case in which the twins are randomly distributed, the diffracted intensity distribution can be modeled because the dimensions can be determined from the CCD images. However, the analysis becomes harder, making the determination of α more complicated.

Image processing of the sample pictures was done with the free, online download software Scion Image,[13] as can be seen in Fig. 5. This processing consisted of four main steps and was done to determine the widths A and C, respectively, of the (100)- and (001)-type ferroelectric domains (twins). The first step was a pixel-by-pixel subtraction of the initial (0-V/mm) image from the final image (600 V/mm) to reveal the morphological differences between the two pictures. The second step smoothed this difference to minimize the interference with the morphological noise at the sample's surface. The third step was a line profile across the image of domains present on the crystal's surface to accentuate the boundaries of the twins. The last step determined the A and C dimensions of the domains with high precision by first reading them in pixels and then converting them to millimeters with the help of the scale attached at the bottom of the sample. The distance R between the line camera detector and the sample was measured with a digital display Vernier caliper.

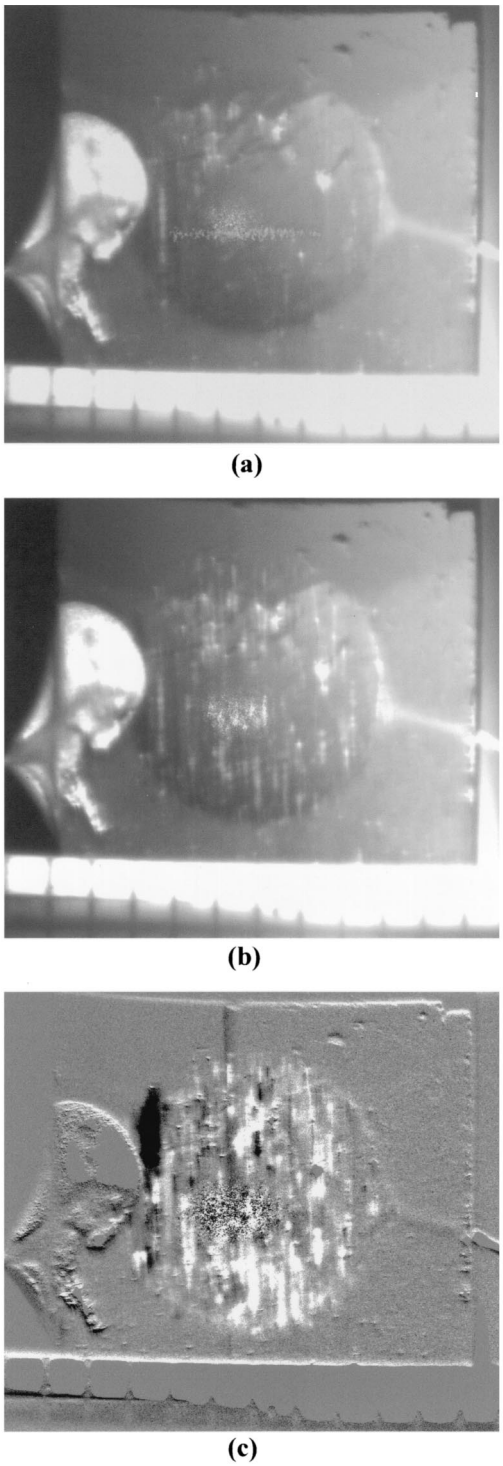

Fig. 5. Images of the surface of the $BaTiO_3$ sample taken with the CCD camera. (a) Sample picture when $E = 0$ V/mm. (b) Sample picture when $E = 600$ V/mm. (c) Sample image after optical processing with Scion Image. The two thin (001) twins are located just at the left and right edges of the dark vertical band that runs through the center and constitutes a steplike portion of the main (100) crystal.

Images from the line camera were imported into a scientific analysis program for conversion into intensity versus position plots. From these plots, we determined the absolute magnitudes of Δx_1 and Δx_2 by first reading them directly in pixels and then transforming them into millimeters using the conversion scale of the graphs. A mathematical software program was used to simulate the theoretical diffracted intensity I as a function of position x. The data obtained here were plotted for convenient comparison of the theoretical plot to the two experimental ones. Finally, after all the necessary values were measured and determined, the value of the angle α was calculated with Eq. (12).

Table 1. Values of Physical Quantities Used in this Paper

Physical Quantity	Value
N	2
λ	0.6328 μm
a	3.992 Å
c	4.036 Å
A	0.1583 mm
C	0.0333 mm
θ_0	45°
x_0	0.0000 mm
x_1	0.0524 mm
x_2	−0.4613 mm
R	110 ± 0.014 mm

4. Results and Discussion

Table 1 shows the values of all the physical quantities given, determined, or measured in this experiment. Figure 6 shows a comparison between the normalized diffracted intensity as a function of position x for the $E = 0$ V/mm experimental curve and for the experimental and theoretical curves at $E = 600$ V/mm. The reduction in the higher-order intensity maxima for the experimental curve as compared with the theoretical curve is mainly due to the fact that the incident laser beam used in the experiment had a Gaussian intensity profile, whereas the theoretical

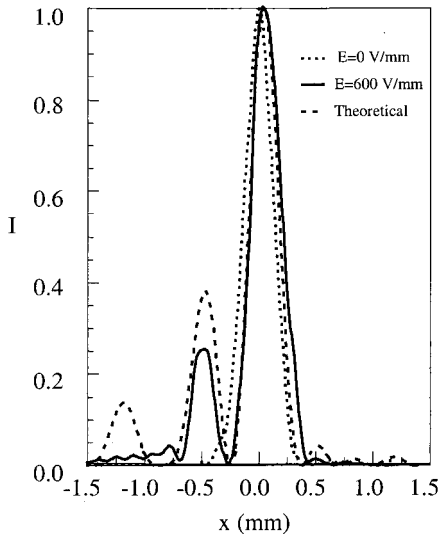

Fig. 6. Plots showing the normalized intensities I versus the position x in different situations specified in the graph's legend.

curve was calculated with a plane wave. The effect of this uneven illumination of the crystal's surface is that the electric fields that superpose to create the diffraction do not have the same amplitude. This, in turn, generates incomplete constructive and destructive interference, thereby substantially reducing the contrast in the pattern. This becomes more pronounced in the higher orders, as can be seen in Fig. 6. However, the intensity level of the secondary diffraction peaks was not crucial in determining α; the important information needed from the experimental I versus x was the two distances, Δx_1 and Δx_2, between the origin and the two main consecutive diffraction peaks.

By substituting the values from Table 1 into Eq. (12), we obtained a value for α of $0.67° \pm 0.05°$. Although A, C, Δx_1, and Δx_2 appear in Eq. (12), each is determined from an image analysis program and shows no variation to four significant figures, so their contribution to the uncertainty is negligible. The largest contribution to the uncertainty in α arises from the denominator in Eq. (12) for the following reason. Because R is at least 3 orders of magnitude larger that any other length parameter, the two terms in the denominator are almost equal. As a result, the denominator becomes small, thereby making α quite sensitive to small uncertainties in R. We determined the uncertainty in α by substituting the two extreme values of R determined from its uncertainty. Although reducing the uncertainty in R would yield a more precise result for α, it is not clear that a more precise measurement of R can be made with our experimental arrangement.

An important point concerning this experiment, however, is the small percentage difference (6.3%) between the experimental and the theoretical values of α. This difference indicates that this simple optical technique is as good a candidate as any of the microscopic techniques, mentioned in Section 1, for determining the twin angle of a $BaTiO_3$ sample.

5. Conclusion

We have measured the twin angle α in $BaTiO_3$, with a 6.3% difference between the experimental and theoretical values, using an optical technique based on Fraunhofer diffraction. A (100), bulk, single crystal of barium titanate with dimensions of 5 mm $\times$ 5 mm $\times$ 1 mm was used as the sample. The twinning was electrically induced, and the detectors were a CCD camera for crystal pictures and a line camera for intensity distribution. Two major advantages of this nondestructive method are low cost and simplicity. This technique can also be advantageous for studying time-resolved formation and evolution of ferroelectric domains. It may also be possible that ferroelectric crystals, such as $BaTiO_3$, might find extra applications in the manufacturing of electrically tuned blazed diffraction gratings used in other research fields such as astrophysics, spectroscopy, and x-ray scattering.

The authors acknowledge support from the Texas Higher Education Coordinating Board Advanced Research Program. We also thank C. L. Chen and X. H. Chen for depositing the gold electrodes on the sample.

References

1. M. V. Klassen-Neklyudova, *Mechanical Twinning of Crystals* (Consultants Bureau, New York, 1964).
2. F. Jona and G. Shirane, *Ferroelectric Crystals* (Pergamon, New York, 1962; reprint, Dover, New York, 1993).
3. S.-I. Hamazaki, F. Shimizu, S. Kojima, and M. Takashige, "AFM observation of 90° domains of $BaTiO_3$ butterfly crystals," J. Phys. Soc. Jpn. **64,** 3660–3663 (1995).
4. M. Takashige, S.-I. Hamazaki, N. Fukurai, F. Shimizu, and S. Kojima, "Atomic force microscope observation of ferroelectrics: barium titanate and Rochelle salt," Jpn. J. Appl. Phys. **35,** 5181–5184 (1996).
5. M. Takashige, S.-I. Hamazaki, N. Fukurai, and F. Shimizu, "Surface morphology of tetragonal $PbTiO_3$ and $BaTiO_3$ observed by atomic force microscopy," J. Phys. Soc. Jpn. **66,** 1848–1849 (1997).
6. S. Balakumar, J. B. Xu, J. X. Ma, S. Ganesamoorthy, and I. H. Wilson, "Surface morphology of ferroelectric domains in $BaTiO_3$ single crystals: an atomic force microscopy study," Jpn. J. Appl. Phys. **36,** 5566–5569 (1997).
7. T. Yamamoto, K. Kawano, M. Saito, and S. Omika, "Surface and domain structure of pure $PbTiO_3$, Mn-doped PbTiO3 and $Pb(Zn_{1/2}Nb_{1/2})_{0.91}Ti_{0.09}O_3$ single crystals by atomic force microscopy," Jpn. J. Appl. Phys. **36,** 6145–6149 (1997).
8. M. Takashige, S.-I. Hamazaki, Y. Takahashi, F. Shimizu, and T. Yamaguchi, "Temperature dependent surface images of $BaTiO_3$ observed by atomic force microscopy," Jpn. J. Appl. Phys. **38,** 5686–5688 (1999).
9. A. L. Gruverman, J. Hatano, and H. Tokumoto, "Scanning force microscopy studies of domain structure in $BaTiO_3$ single crystals," Jpn. J. Appl. Phys. **36,** 2207–2211 (1997).
10. G. A. Schneider and J. M. Saldaña, "Investigations of domain-structure and motion in ferroelectric ceramics by scanning force microscopy," http://www.tu-harburg.de/gkjms/english.htm.
11. G. Tarrach, P. Lagos, R. Hermans, Z. F. Schlaphof, Ch. Loppacher, and L. M. Eng, "Nanometer spot allocation for Raman spectroscopy on ferroelectrics by polarization and piezoresponse force microscopy," Appl. Phys. Lett. **79,** 3152–3154 (2001).
12. U. Klemradt, M. Aspelmeyer, L. T. Wood, and S. C. Moss, "An experimental method to investigate the structure and kinetics of patterned surfaces using laser light diffraction," Rev. Sci. Instrum. **73,** 108–113 (2002).
13. Scion Corporation, 82 Worman's Mill Court, Suite H, Frederick, Md. 21701, http://www.scioncorp.com.

Method for measuring off-diagonal Kerr coefficients by using polarized light transmission

Mike Melnichuk and Lowell T. Wood

Department of Physics, University of Houston, Houston, Texas 77204-5005

Received May 7, 2004; revised manuscript received July 2, 2004; accepted August 30, 2004

We report a method for measuring the off-diagonal coefficients of the quadratic electro-optic (Kerr) tensor by using polarized light transmission. The method relies on designing an experimental configuration in which the linear electro-optic (Pockels) effect does not contribute to the data. Our method can be used to obtain off-diagonal Kerr coefficients for all but two of the 20 crystal point groups for which the Pockels effect and the Kerr effect coexist. Our theoretical model includes effects from transmission, multiple reflections, and electrostriction but neglects absorption in the crystal. To verify the method, we used it to measure the R_{12} and R_{13} Kerr coefficients for a (100)-type single crystal of ferroelectric barium titanate ($BaTiO_3$) at room temperature (23.5°). To our knowledge, this is the first time this method has been used and the first time these coefficients have been measured for the unclamped crystal in the tetragonal state. The mean values obtained with this method are $R_{12} = -3.5 \pm 0.3 \times 10^{-17}\,m^2/V^2$ and $R_{13} = -8.0 \pm 0.7 \times 10^{-17}\,m^2/V^2$.

OCIS codes: 190.3270, 160.2260, 260.1180, 160.1190, 230.4110.

1. INTRODUCTION

Electro-optic effects belong to the larger class of nonlinear optics phenomena.[1] In nonlinear optics, the coefficients are either calculated from a microscopic theory or experimentally determined.[2] Because a coherent microscopic theory of ferroelectrics is lacking, and the only one available at present is a phenomenological (free-energy) theory,[3–18] the only way to gain extra information about some of the electro-optic coefficients is to determine them experimentally.

The electro-optic effect is the change of the index ellipsoid of a crystal with the application of an electric field. For crystals with inversion symmetry (12 point groups), the linear electro-optic (Pockels) effect does not exist; the quadratic electro-optic (Kerr) effect is the dominant one. In crystals lacking inversion symmetry (noncentrosymmetric crystals), both the linear and the quadratic effects are simultaneously possible, with the Pockels effect being the dominant one. If one designs an experiment configured in such a way that the individual products $r_{ij}E_j = 0$ with $i, j = 1, 2, 3$, then the Pockels effect does not contribute to the results, and the Kerr effect provides the primary contribution to the data. In that case the r_{ij} are the first-order electro-optic coefficients, and the E_j are the components of the externally applied electric field. The Kerr coefficients can be extracted by use of the theory presented in Section 2.

To test our method, we measured the R_{12} and R_{13} Kerr coefficients for barium titanate in the tetragonal state, where both the Pockels effect and the Kerr effect are present. At temperatures above 120 °C (Curie temperature), barium titanate is in the paraelectric state, which is cubic with point group symmetry $m3m$. The quadratic electro-optic effect, which is the main one for this phase, induces changes in the refractive index[19–22] of the order of 10^{-4}–10^{-3}.

Between −5 °C and 120 °C, $BaTiO_3$ is in the ferroelectric state, which is tetragonal with point group symmetry $4mm$; in this phase the inversion symmetry vanishes owing to the appearance of a spontaneous polarization. The linear electro-optic effect, which is the dominant one now, is, in fact, a particular case of a quadratic electro-optic effect biased by the spontaneous polarization[23] $\mathbf{P}_s$.

The difference between the primary diagonal and primary off-diagonal quadratic electro-optic coefficients has been measured before for $BaTiO_3$; but to the authors' knowledge, this has been done only in the paraelectric, cubic ($m3m$) state. Recent scientific literature[24–28] concerning linear combinations or individual measured values of any of the Kerr coefficients for barium titanate shows nothing for the ferroelectric, tetragonal ($4mm$) state. In fact, there are few, if any, values reported for off-diagonal coefficients in any of the noncentrosymmetric crystals.[26–28]

We present an optical technique for measuring off-diagonal Kerr coefficients in all but two of the 20 noncentrosymmetric crystal point groups (triclinic 1 and the trigonal 3). We apply the method to measure R_{12} and R_{13}, for ferroelectric $BaTiO_3$ at room temperature ($T = 23.5$ °C) and wavelength $\lambda = 632.8$ nm.

2. THEORY

This section is divided into two parts. In the first part we demonstrate how contributions from the Pockels effect were avoided. In the second part we deduce the system of nonlinear equations from which the off-diagonal Kerr coefficients are extracted numerically from the experimental data.

For the most general case (a biaxial crystal), the equation of the initial index ellipsoid (initial indicatrix) at a zero electric field is given by

$$\frac{x^2}{n_1^2} + \frac{y^2}{n_2^2} + \frac{z^2}{n_3^2} = 1. \tag{1}$$

With the application of an external electric field

$$\mathbf{E} = E_1\hat{\mathbf{x}} + E_2\hat{\mathbf{y}} + E_3\hat{\mathbf{z}}, \tag{2}$$

the equation of the new index ellipsoid, in the same (x, y, z)-coordinate system, takes the new form

$$\frac{x^2}{n_1'^2} + \frac{y^2}{n_2'^2} + \frac{z^2}{n_3'^2} + \frac{2yz}{n_4'^2} + \frac{2xz}{n_5'^2} + \frac{2xy}{n_6'^2} = 1 \tag{3}$$

(see Fig. 1). There always exists a principal system of Cartesian axes (x'', y'', z'') in which Eq. (3) can be written in the canonical form

$$\frac{x''^2}{n_1''^2} + \frac{y''^2}{n_2''^2} + \frac{z''^2}{n_3''^2} = 1. \tag{4}$$

The intersection of this new indicatrix with the yz, xz, and xy planes gives three new ellipses, which are rotated with respect to the initial ellipses in these planes, with rotation angles ω_4, ω_5, and ω_6, respectively. These angles are calculated from the formulas

$$\tan(2\omega_4) = \frac{2r_{4j}E_j}{(1/n_2'^2) - (1/n_3'^2)}, \tag{5}$$

$$\tan(2\omega_5) = \frac{2r_{5j}E_j}{(1/n_1'^2) - (1/n_3'^2)}, \tag{6}$$

$$\tan(2\omega_6) = \frac{2r_{6j}E_j}{(1/n_1'^2) - (1/n_2'^2)}, \tag{7}$$

with $0° \leqslant |\omega_4|, |\omega_5|, |\omega_6| \leqslant 45°$, and assuming only the first-order electro-optic effect. To change from tensor to matrix notation, in Eqs. (5)–(7), we used Nye's suffix abbreviation[29]:

$$(11) \rightarrow 1; \quad (22) \rightarrow 2; \quad (33) \rightarrow 3;$$

$$(23), (32) \rightarrow 4; \quad (13), (31) \rightarrow 5;$$

$$(12), (21) \rightarrow 6.$$

With this notation, the Pockels and Kerr expressions connecting the new refractive indexes (n'), the initial ones (n), and the three components (E_1, E_2, E_3) of the applied electric field in the (x, y, z) system of coordinates can be explicitly written as

$$\frac{1}{n_i'^2} = \frac{1}{n_i^2} + r_{ij}E_j + R_{i(kl)}E_kE_l, \tag{8}$$

with $1/n_4 = 1/n_5 = 1/n_6 = 0$; $j, k, l = 1, 2, 3$; $i, (kl) = 1, 2,...,6$. The r_{ij} and $R_{i(kl)}$ are the linear and the quadratic electro-optic tensor's components, respectively, and (kl) follows Nye's notation. Both the Pockels and Kerr coefficients are dependent on the dielectric constants of the material, which in turn are functions of temperature and applied electric fields. Moreover, the Kerr fourth-order tensor is symmetric ($R_{pq} = R_{qp}$, with $p, q = 1, 2,...,6$).

To calculate how the indexes of refraction in the initial (x, y, z) coordinate system change with the application of the electric field, one intersects the new indicatrix with the Ox, Oy, or Oz axes to obtain

$$\frac{1}{n_1'^2} = \frac{1}{n_1^2} + r_{1j}E_j + R_{1(kl)}E_kE_l, \tag{9}$$

$$\frac{1}{n_2'^2} = \frac{1}{n_2^2} + r_{2j}E_j + R_{2(kl)}E_kE_l, \tag{10}$$

$$\frac{1}{n_3'^2} = \frac{1}{n_3^2} + r_{3j}E_j + R_{3(kl)}E_kE_l. \tag{11}$$

In Eqs. (9)–(11), note that if the individual products $r_{ij}E_j = 0$ with $i, j = 1, 2, 3$, then the linear electro-optic effect will have no effect on the magnitude of the new refractive indexes corresponding to the initial x, y, and z directions. Geometrically, the above statement has a simple but very interesting formulation. If higher-order electro-optic effects are not considered, then every time $r_{ij}E_j = 0$ for $i, j = 1, 2, 3$, the newly generated index ellipsoid will acquire a shape and direction such that its intersection points with the original (x, y, z) Cartesian system of coordinates will always coincide with the intersection points that the original index ellipsoid makes with that same coordinate system; these intersection points are invariant to the coordinate transformation. A physical interpretation of the above statement is that any polarized light wave passing at normal incidence through any crystal in which the components of the applied electric field satisfy the condition $r_{ij}E_j = 0$ for $i, j = 1, 2, 3$, will have no contribution from the Pockels effect. In particular, for a tetragonal $BaTiO_3$ crystal, linearly polarized light in a direction parallel to either the Ox, Oy, or Oz axes does not register any change in the indexes of refraction due to the Pockels effect. For the above particular configuration, the linear electro-optic effect cannot be detected. For other crystal structures, the above condition can be satisfied by changing either the crystal orientation or the direction of the applied electric field.

It is this observation, along with its physical interpretation, that allows us to determine the values for the R_{12} and R_{13} Kerr coefficients. For barium titanate, which is a negative uniaxial crystal in the tetragonal state, $n_1 = n_2 = n_o$ are the ordinary indexes of refraction and $n_3 = n_e$ is the extraordinary index. Their values[24] at $\lambda = 632.8$ nm are $n_o = 2.413$, and $n_e = 2.361$.

Using the general convention[2,30] that the z axis should always be considered along the direction of the spontaneous polarization $\mathbf{P}_s$, the linear and quadratic electro-optic equations in the tetragonal state can be expressed in a condensed matrix format as

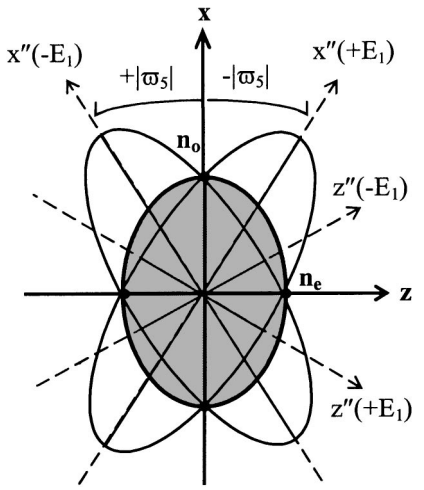

Fig. 1. Greatly exaggerated schematic of the refraction index ellipses in the xz plane and their corresponding rotation angles for the case with zero, positive, or negative applied electric field. The electric field is parallel to the x axis; the y axis points upward out of the paper. The Kerr effect is not considered. The ellipses associated with the nonzero electric fields and the one corresponding to a zero electric field intersect the original axes in the same points (for individual products $r_{ij}E_j = 0, i, j = 1, 2, 3$); for this experimental configuration the refraction indexes read by the probing light at normal incidence on the $BaTiO_3$ sample do not change because of the Pockels effect when the electric field is applied in either the $+x$ or the $-x$ direction.

$$\begin{pmatrix} 1/n_1'^2 \\ 1/n_2'^2 \\ 1/n_3'^2 \\ 1/n_4'^2 \\ 1/n_5'^2 \\ 1/n_6'^2 \end{pmatrix} = \begin{pmatrix} 1/n_o^2 \\ 1/n_o^2 \\ 1/n_e^2 \\ 0 \\ 0 \\ 0 \end{pmatrix} + \begin{bmatrix} 0 & 0 & r_{13} \\ 0 & 0 & r_{13} \\ 0 & 0 & r_{33} \\ 0 & r_{51} & 0 \\ r_{51} & 0 & 0 \\ 0 & 0 & 0 \end{bmatrix} \begin{pmatrix} E_1 \\ E_2 \\ E_3 \end{pmatrix} + \begin{bmatrix} R_{11} & R_{12} & R_{13} & 0 & 0 & 0 \\ R_{12} & R_{11} & R_{13} & 0 & 0 & 0 \\ R_{13} & R_{13} & R_{33} & 0 & 0 & 0 \\ 0 & 0 & 0 & R_{44} & 0 & 0 \\ 0 & 0 & 0 & 0 & R_{44} & 0 \\ 0 & 0 & 0 & 0 & 0 & R_{66} \end{bmatrix} \times \begin{pmatrix} E_1^2 \\ E_2^2 \\ E_3^2 \\ E_2E_3 \\ E_1E_3 \\ E_1E_2 \end{pmatrix}. \quad (12)$$

According to the general observation above, if the electric field applied to the tetragonal $BaTiO_3$ sample has only an x component (E_1), and the second- and higher-order effects are ignored, then the new indexes of refraction, as detected by the normal incident light, will not change because of the Pockels effect (see Fig. 1). The only thing that the linear electro-optic effect does in this case is to modify the form and inclination of the new indicatrix in such a way that its corresponding Cartesian x'', z'' axes are rotated with respect to the original x, z axes by an angle ϖ_5 given by

$$\tan(2\varpi_5) = \frac{2r_{51}E_1}{(1/n_o^2) - (1/n_e^2)}. \quad (13)$$

In the second part of this theoretical section, we deduce the system of nonlinear equations that relate the two relative intensities of the transmitted orthogonally polarized light beams to the applied electric field and to the two off-diagonal Kerr coefficients at room temperature.

The theoretical model associated with the experiment is schematically shown in Fig. 2. Below are the consecutive physical steps through the optical system and their corresponding equations. After exiting the 45° polarizer, the two orthogonal polarizations have the same amplitude given by

$$A_{y0} = A_{z0} = A_0. \quad (14)$$

After passing through the bulk of the crystal, the two transmitted amplitudes change into

$$A_{y1} = t_y A_{y0}, \quad (15)$$

$$A_{z1} = t_z A_{z0}, \quad (16)$$

with the corresponding transmission coefficients[31]

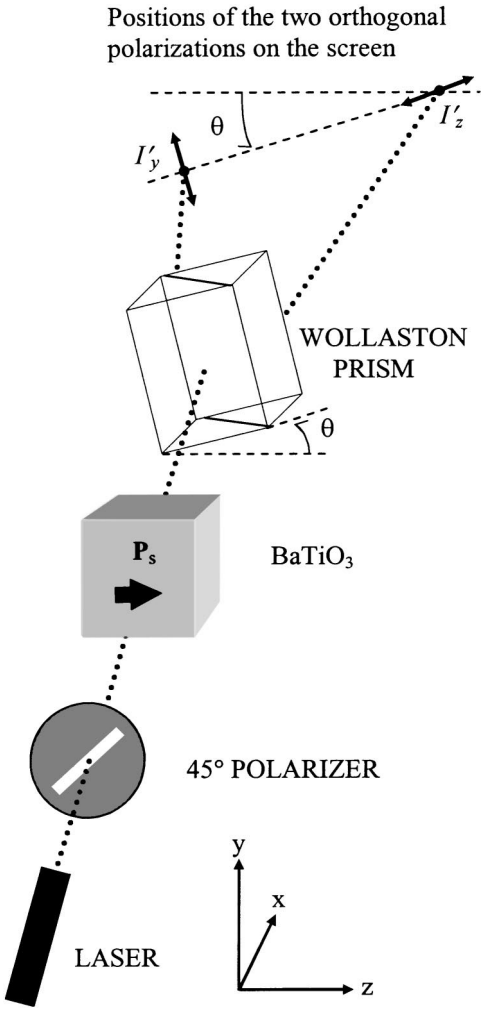

Fig. 2. Simple schematic of our optical amplitude modulation system.

$$t_y = \frac{(1 - r_y^2)\exp(-i\varphi_y)}{1 - r_y^2\exp(-2i\varphi_y)} = \frac{[(1 - r_y^2)^2\cos(\varphi_y)] - i[(1 - r_y^4)\sin(\varphi_y)]}{(1 + r_y^4) - 2r_y^2\cos(2\varphi_y)}, \quad (17)$$

$$t_z = \frac{(1 - r_z^2)\exp(-i\varphi_z)}{1 - r_z^2\exp(-2i\varphi_z)} = \frac{[(1 - r_z^2)^2\cos(\varphi_z)] - i[(1 - r_z^4)\sin(\varphi_z)]}{(1 + r_z^4) - 2r_z^2\cos(2\varphi_z)}. \quad (18)$$

$$I_y = A_0^2\left[T_y\cos^2(\theta) + T_z\sin^2(\theta) - \frac{1}{2}T_{yz}\sin(2\theta)\right], \quad (25)$$

$$I_z = A_0^2\left[T_z\cos^2(\theta) + T_y\sin^2(\theta) + \frac{1}{2}T_{yz}\sin(2\theta)\right], \quad (26)$$

with

$$T_y = |t_y|^2 = \frac{(1 - r_y^2)^2}{(1 + r_y^4) - 2r_y^2\cos(2\varphi_y)}, \quad (27)$$

$$T_z = |t_z|^2 = \frac{(1 - r_z^2)^2}{(1 + r_z^4) - 2r_z^2\cos(2\varphi_z)}, \quad (28)$$

$$T_{yz} = t_y t_z^* + t_y^* t_z = 2\frac{(1 - r_y^2)(1 - r_z^2)[(1 + r_y^2 r_z^2)\cos(\Delta\varphi) - (r_y^2 + r_z^2)\cos(\varphi_y + \varphi_z)]}{[(1 + r_y^4) - 2r_y^2\cos(2\varphi_y)][(1 + r_z^4) - 2r_z^2\cos(2\varphi_z)]}, \quad (29)$$

These transmission coefficients take into account the effect of multiple reflections at the two faces of the crystal. The r_y, r_z are the Fresnel reflection coefficients at normal incidence; they are related to the indexes of refraction n_y, n_z in the following way:

$$r_y = \frac{n_y - 1}{n_y + 1}, \quad (19)$$

$$r_z = \frac{n_z - 1}{n_z + 1}. \quad (20)$$

For $BaTiO_3$, $n_y = n_2'$ and $n_z = n_3'$, where n_2' and n_3' are given by Eq. (12).

The φ_y, φ_z are the phases aquired by the two polarized waves after passing through the sample and are given by

$$\varphi_y = (2\pi/\lambda)n_y l_x, \quad (21)$$

$$\varphi_z = (2\pi/\lambda)n_z l_x, \quad (22)$$

with l_x being the length of the crystal in the direction of the incident light. In our model we do not take into account the phenomenon of light absorption through the barium titanate slab.[32]

After exiting the crystal sample, the light then passes through a Wollaston prism that is rotated by an angle θ in the plane normal to the incident direction. The final forms for the orthogonally polarized amplitudes of light after exiting our optical amplitude modulation system are

$$A_y = A_{y1}\cos(\theta) - A_{z1}\sin(\theta), \quad (23)$$

$$A_z = A_{z1}\cos(\theta) + A_{y1}\sin(\theta). \quad (24)$$

The light intensities are calculated by multiplying the above electromagnetic amplitudes (A_y, A_z) by their corresponding complex conjugates (A_y^*, A_z^*). From the results of Eqs. (14)–(24), the transmitted intensities of the two orthogonally polarized waves are

$$\Delta\varphi = \varphi_z - \varphi_y. \quad (30)$$

The amplitude modulated signal oscillates with a frequency directly proportional to the phase difference $\Delta\varphi$. On top of this signal, there are many small interference fringes generated by the multiple reflections at the two faces of the crystal; their frequencies are directly proportional to the phases φ_y and φ_z. To calculate the net effect of these rapid fringes on the amplitude of the modulated signal, we average the transmissivities T_y, T_z and the mixed term T_{yz} over a 2π interval for each of the two phases φ_y and φ_z. Considering the $\Delta\varphi$ as an independent variable, we obtain

$$\langle T_y\rangle = \frac{1}{(2\pi)^2}\int_0^{2\pi}\int_0^{2\pi} T_y(\varphi_y)\mathrm{d}\varphi_y\mathrm{d}\varphi_z = \frac{1 - r_y^2}{1 + r_y^2}, \quad (31)$$

$$\langle T_z\rangle = \frac{1}{(2\pi)^2}\int_0^{2\pi}\int_0^{2\pi} T_z(\varphi_z)\mathrm{d}\varphi_y\mathrm{d}\varphi_z = \frac{1 - r_z^2}{1 + r_z^2}, \quad (32)$$

$$\langle T_{yz}\rangle = \frac{1}{(2\pi)^2}\int_0^{2\pi}\int_0^{2\pi} T_{yz}(\varphi_y, \varphi_z)\mathrm{d}\varphi_y\mathrm{d}\varphi_z = 2\frac{(1 + r_y^2 r_z^2)\cos(\Delta\varphi)}{(1 + r_y^2)(1 + r_z^2)}. \quad (33)$$

The average transmitted intensities for the two polarizations ($\langle I_y\rangle$, $\langle I_z\rangle$) become

$$\langle I_y\rangle = A_0^2\left[\langle T_y\rangle\cos^2(\theta) + \langle T_z\rangle\sin^2(\theta) - \frac{1}{2}\langle T_{yz}\rangle\sin(2\theta)\right], \quad (34)$$

$$\langle I_z\rangle = A_0^2\left[\langle T_z\rangle\cos^2(\theta) + \langle T_y\rangle\sin^2(\theta) + \frac{1}{2}\langle T_{yz}\rangle\sin(2\theta)\right]. \quad (35)$$

Because the tensor for the inverse piezoelectric effect has the same symmetry properties as the Pockels tensor for this particular configuration, the inverse piezoelectric effect does not contribute to the change in the length of the crystal in the direction of light propagation. It is the electrostriction effect that causes changes in l_x of the form

$$l_x = l_{x0}(1 + s_x), \tag{36}$$

where l_{x0} is the dimension of the crystal in the x direction with no external electric field applied and s_x is the electrostrictive strain. For tetragonal $BaTiO_3$, the value of the electrostrictive strain was obtained from a previous graph of the strain versus the electric field (with no external stress) obtained by Burcsu and co-workers[33,34] for the same type of $BaTiO_3$ crystal as ours, having the same specifications and even purchased from the same company.[35] The electrostrictive strain has an average value of $s_x = 0.10 \pm 0.05\%$ for electric fields between 1×10^5 V/m and 7×10^5 V/m. The value of the crystal's width is $l_{x0} = 1$ mm, and it was provided by the manufacturer.[35]

The net relative light intensities for the two polarizations, $\langle I_{yr} \rangle$ and $\langle I_{zr} \rangle$, are calculated by dividing the value of each average transmitted intensity, $\langle I_y \rangle$ and $\langle I_z \rangle$, measured at a nonzero electric field ($E \neq 0$ V/m), by the initial value of the same corresponding intensity I_{y0}, I_{z0} when $E = 0$ V/m. The results are given by

$$\langle I_{yr} \rangle = \frac{\langle I_y \rangle}{I_{y0}} = \frac{\langle T_y \rangle \cos^2(\theta) + \langle T_z \rangle \sin^2(\theta) - (1/2)\langle T_{yz} \rangle \sin(2\theta)}{T_{y0} \cos^2(\theta) + T_{z0} \sin^2(\theta) - (1/2) T_{(yz)0} \sin(2\theta)}, \tag{37}$$

$$\langle I_{zr} \rangle = \frac{\langle I_z \rangle}{I_{z0}} = \frac{\langle T_z \rangle \cos^2(\theta) + \langle T_y \rangle \sin^2(\theta) + (1/2)\langle T_{yz} \rangle \sin(2\theta)}{T_{z0} \cos^2(\theta) + T_{y0} \sin^2(\theta) + (1/2) T_{(yz)0} \sin(2\theta)}, \tag{38}$$

where T_{y0}, T_{z0}, and $T_{(yz)0}$ are the transmission coefficients and the mixed transmission term in the initial state of the crystal, before the application of an electric field. For normalization purposes, so that $\langle I_{yr} \rangle \to 1$ and $\langle I_{zr} \rangle \to 1$ when $E_1 \to 0$ and $s_x \to 0$, we chose the denominators in Eqs. (37) and (38) to have a form analogous to their corresponding numerators when E_1 and s_x are zero.

3. EXPERIMENT

The experimental design is schematically shown in Fig. 3; all data were collected at a temperature of 23.5 °C. The sample was an unclamped 5 mm × 5 mm × 1 mm, two-face-polished, (100)-oriented, single crystal of barium titanate. It was mounted with the spontaneous polarization $\mathbf{P}_s$ in the z direction. A pair of electrodes 3 mm in diameter were created by sputtering a 20-nm thin layer of gold on the 5 mm × 5 mm opposite faces of the sample. The connection between these electrodes and the electrical cables from a high-voltage power supply (PS) was done through a pair of thin gold wires (GW), which were permanently attached to the sample's electrodes with a colloidal silver paste solution. The front surface of the $BaTiO_3$ crystal was illuminated with an incandescent lamp (IL), making it visible to a CCD camera (BASLER A101p, 1300H × 1030V pixels, pixel size 6.7 μm × 6.7 μm).

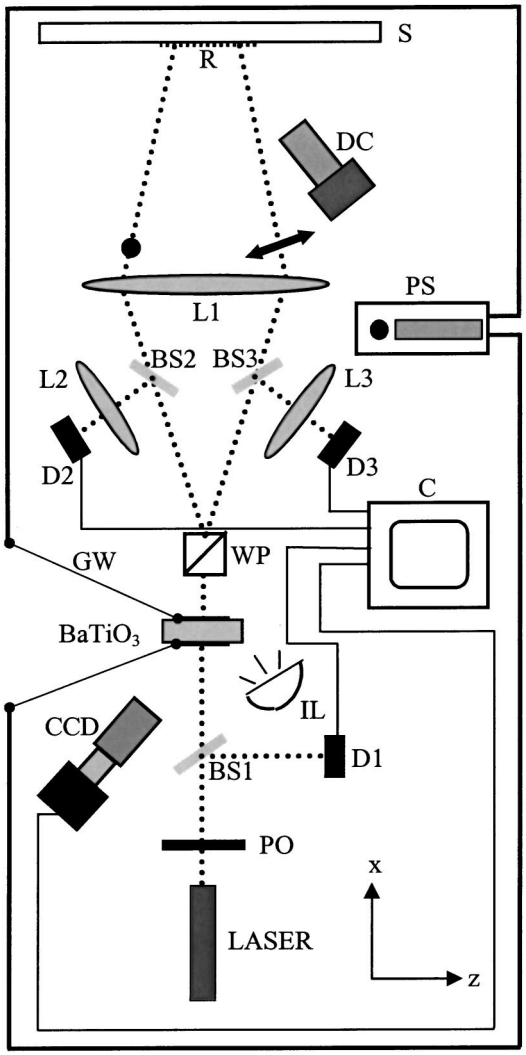

Fig. 3. Schematic of the experimental setup; the y axis points upward out of the paper. S, screen; R, ruler; DC, digital camera; L1, L2, L3, lenses; BS1, BS2, BS3, beam splitters; D1, D2, D3, light intensity detector; GW, gold wire; PS, power supply; WP, Wollaston prism; C, computer; CCD, camera; IL, incandescent lamp; PO, 45° linear polarizer.

A 0.5-mW He–Ne laser beam, with wavelength $\lambda = 632.8$ nm and a diameter of 0.48 mm at the $1/e^2$ points, was transmitted through the crystal after being split by a beam splitter (BS1). One part of the incident beam went into a light intensity detector (D1), which was used to monitor changes in the magnitude of the incident beam's intensity (I_m). Before reaching the crystal, the incoming light was linearly polarized at 45° relative to $\mathbf{P}_s$ with a linear polarizer (PO). After passing through the crystal, the transmitted beam was divided with a Wollaston prism (WP) into two beams of light having mutually perpendicular polarizations. The prism was rotated coun-

terclockwise by an angle $\theta = 15°$ in the plane normal to the direction of the light's propagation (see Fig. 2). The rotated Wollaston prism was the novel design feature that differentiated our amplitude modulator from the standard ones found in the optical literature[36–45] because it allowed modulation of both orthogonally polarized waves at the same time. This simultaneous amplitude modulation characteristic is expressed in mathematical form in Eqs. (23) and (24).

Each of those two orthogonally polarized beams was then further separated into two lower-intensity ones with the help of a set of beam splitters (BS2, BS3). For each of these new lower-intensity beams, part of it was focused by a convergent lens (L2 or L3) into a light intensity detector (D2 or D3) while the other part was passed through a common convergent lens (L1) onto a screen (S) having a thin, millimeter-type ruler (R) attached to it. All data were collected and processed with a computer (C) (see Fig. 3).

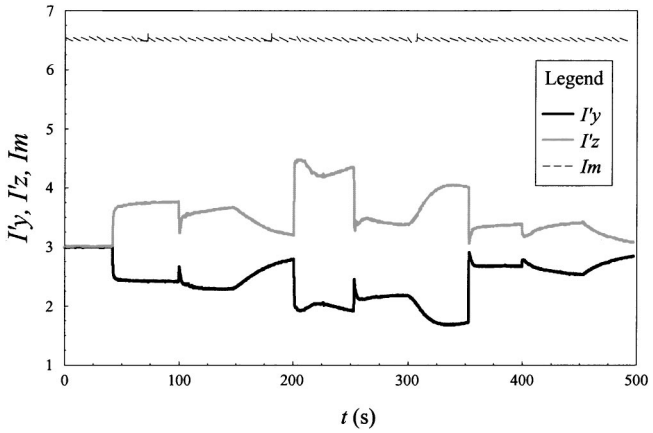

Fig. 4. Plot of I'_y, I'_z, and I_m versus time for the first experimental trial. The applied electric field (E_1) across the $BaTiO_3$ sample was switched in a steplike fashion approximately every 50 s for 500 s. The values of the electric voltage taken in chronological order are 0, +400, −400, 0, +600, −600, 0, +200, −200, 0 V.

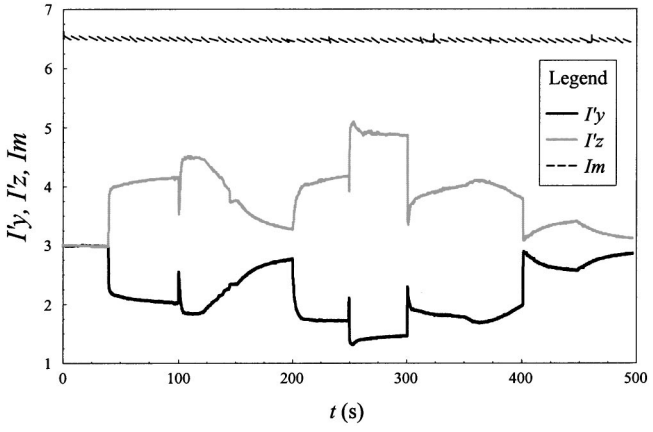

Fig. 5. Plot of I'_y, I'_z, and I_m versus time for the second experimental trial. The applied electric field (E_1) across the $BaTiO_3$ sample was switched in a steplike fashion approximately every 50 s for 500 s. The values of the electric voltage taken in chronological order are 0, −400, +400, 0, −600, +600, −600, 0, +200, 0 V. This time the −400 V voltage drop on the sample was kept on for only ~20 s.

Data were collected in the following way. The electric field E_1 across the sample was varied in a steplike fashion approximately every 50 s for 500 s; this was done manually for positive, zero, and negative values of the electrical potential with the help of a toggle switch. The light intensity values collected by the three detectors, D1, D2, and D3, were acquired every 0.02 s for 500 s with the data collection software, Vernier LabPro 2.2.1. Detector D1 measured the monitor beam's intensity (I_m), D2 the intensity polarized along the y axis of the crystal (I'_y), and D3 the intensity polarized along the z axis (I'_z). These three intensity values were plotted versus time with the software PSI-Plot (Version 7); see Figs. 4 and 5.

The CCD camera acquired images of the crystal's surface every second for 500 s, and pictures of the transmitted light's intensity patterns on the screen were taken manually every 25 s for all 500 s with a Sony digital camera (Fig. 3, DC) having the specifications XGA, 1024 × 768 pixels. The CCD camera was used to monitor changes at the crystal's surface, and the digital camera was employed for capturing any change in the intensity pattern of light when the external electric field was applied across the sample. Some striking changes at the surface of the sample, due to polysynthetic twinning,[46] were detected by the CCD camera when the voltage was changed near the values of ±600 V/mm. These variations in the surface morphology of the crystal led to a more diffuse light transmission, especially for the light polarized in the z' direction. This was confirmed by the pictures of the light's spatial distribution on the screen (S) taken with the digital camera. We will devote more time to these changes when we will look at the evolution of light intensity with time for different applied voltages.

4. RESULTS AND DISCUSSION

Figures 4 and 5 show the change in the orthogonally polarized intensities as a function of time for various values of the applied electric field (E_1). The fact that the value of the polarized intensity I'_y (or I'_z) never goes above (or below) the zero-voltage initial value I'_{y0} (or I'_{z0}), when the sign of the electric field is changed indicates a quadratic electro-optic effect in barium titanate.

After processing the data, we always chose the time-average of the two light intensities (I'_y, I'_z), every time a nonzero electric field was applied, and divided these values by the values of the initial (time-average) intensities (I'_{y0}, I'_{z0}). This procedure gave us the relative measured intensities of light (I'_{yr}, I'_{zr}) for different values of the electric field (E_1). These sets of measured values, with their uncertainties, were substituted (I'_{yr} for $\langle I_{yr}\rangle$, and I'_{zr} for $\langle I_{zr}\rangle$) in Eqs. (37) and (38), from which a corresponding set of values for R_{12} and R_{13}, and their uncertainties, was numerically extracted every time. The working range of the light amplitude modulator was taken to be $-\pi/2 \leqslant \Delta\varphi \leqslant \pi/2$. The time averages and uncertainties (standard deviations) for the relative light intensities were calculated with the software PSI-Plot (Version 7). The time average and the two extreme values for each of these relative intensities were substituted into Eqs. (37) and (38), giving us the corresponding average and uncertainty values for the Kerr coefficients. These numerical

Table 1. Orthogonally Polarized Intensities I'_{yr}, I'_{zr} and Off-Diagonal Kerr Coefficients R_{12}, R_{13} for Externally Applied Electric Fields E_1, First Experimental Trial

$E_1(10^3$ V/m)	I'_{yr}	I'_{zr}	$R_{12}(10^{-17}$ m^2/V^2)	$R_{13}(10^{-17}$ m^2/V^2)
+400	0.80 ± 0.02	1.23 ± 0.03	−3.51 ± 0.11	−7.82 ± 0.13
−400	0.78 ± 0.02	1.20 ± 0.05	−3.59 ± 0.11	−7.92 ± 0.31
+600	0.66 ± 0.04	−3.67 ± 0.23	1.44 ± 0.08	−7.58 ± 0.49
−600	0.71 ± 0.02	1.15 ± 0.03	−3.70 ± 0.11	−6.26 ± 0.19
+200	0.88 ± 0.01	1.11 ± 0.01	−3.43 ± 0.06	−8.19 ± 0.07
−200	0.85 ± 0.02	1.11 ± 0.02	−3.42 ± 0.11	−8.21 ± 0.13
Trial 1 Average	—	—	−3.5 ± 0.3	−7.9 ± 0.5

Table 2. Orthogonally Polarized Intensities I'_{yr}, I'_{zr} and Off-Diagonal Kerr Coefficients R_{12}, R_{13} for Externally Applied Electric Fields E_1, Second Experimental Trial

$E_1(10^3$ V/m)	I'_{yr}	I'_{zr}	$R_{12}(10^{-17}$ m^2/V^2)	$R_{13}(10^{-17}$ m^2/V^2)
−400	0.70 ± 0.03	1.37 ± 0.03	−3.46 ± 0.17	−8.07 ± 0.19
+400	0.61 ± 0.02	1.50 ± 0.02	−3.43 ± 0.11	−8.16 ± 0.13
−600	0.57 ± 0.02	1.38 ± 0.03	−3.53 ± 0.11	−7.75 ± 0.19
+600	0.47 ± 0.04	1.67 ± 0.06	−3.47 ± 0.23	−8.02 ± 0.37
−600	0.61 ± 0.02	1.31 ± 0.03	−3.54 ± 0.11	−7.73 ± 0.19
+200	0.87 ± 0.02	1.13 ± 0.02	−3.41 ± 0.11	−8.26 ± 0.13
Trial 2 Average	—	—	−3.4 ± 0.2	−8.1 ± 0.4

values were obtained with the mathematical software MathCAD 2001i. Tables 1 and 2 summarize the results for the calculated values (R_{12}, R_{13}) and their corresponding uncertainties. The mean values are the overall arithmetical averages of these coefficients for both trials, with the exception of the set of values contained in the fourth row of the first trial (−600 V/mm). The twinning phenomenon, mentioned in Section 3, generates a diffuse reflection of light at the two end surfaces of the sample, leading, in this case, to unreliable values for the calculated Kerr coefficients.

One noteworthy feature about the results is that in each of the two experiments the values of the two off-diagonal Kerr coefficients are different for applied electric fields that have the same magnitude but opposite directions. This is because R_{12} and R_{13} are functions of dielectric constants that, in ferroelectrics, depend nonlinearly on the applied external electric fields.

5. CONCLUSION

We have shown a general method for measuring the off-diagonal coefficients of the quadratic electro-optic (Kerr) tensor and verified its usefulness by determining the two off-diagonal Kerr coefficients, $R_{12} = -3.5 \pm 0.3 \times 10^{-17}$ m^2/V^2 and $R_{13} = -8.0 \pm 0.7 \times 10^{-17}$ m^2/V^2 for a (100), 5 mm × 5 mm × 1 mm, single crystal of $BaTiO_3$. The method relies on selecting an experimental configuration in which the individual products $r_{ij}E_j = 0$ with i, $j = 1, 2, 3$. Unlike other methods,[36–45] our method treats multiple reflections at the two faces of the sample, light transmission through the crystal, and electrostriction. Our method can be used to measure off-diagonal Kerr coefficients on 18 of the 20 crystal point groups in which the Pockels effect and the Kerr effect coexist.

The values for these two quadratic electro-optic coefficients were numerically extracted from the above-mentioned set of nonlinear equations [Eqs. (37) and (38)]. The uncertainties result primarily from nonlinear dielectric behavior with the electric field, which is a common phenomenon in every ferroelectric crystal.

The fact that the two intensities I'_y and I'_z can be associated with the symbols **1** and **0** of Boolean algebra might make it possible for the working principle of this light modulator to find some applications in the improvement or design of new optical binary devices that are so needed in the important technological field of information processing optical devices (optical computers).

Using this technique, one can monitor the changes in the optical coefficients of crystals under different external conditions, i.e., electric or magnetic field and pressure and temperature variations. These measurements can provide the physics community with a new window into the process of symmetry change occurring in crystals immediately after they are subjected to an external stress. Furthermore, the knowledge gained from observing the time evolution of crystal behavior could also be used to improve the state of theoretical modeling associated with the dynamics of phase transitions in some of these crystals.

As the two graphs (Figs. 4 and 5) show, a curious behavior of the light intensities as functions of time ($I'_{yr}(t)$, $I'_{zr}(t)$) was detected every time the applied electric field was changed. The authors have not seen these effects discussed in the scientific literature to date. We suspect that some of these light transients are caused by the change in the indexes of refraction caused by a certain relaxation in the crystal's polarization once the electric stress has been temporarely removed. A more concrete and detailed study of the connection between this tran-

sient behavior and time-dependent phenomena in barium titanate has been submitted for publication.[47]

ACKNOWLEDGMENTS

The authors acknowledge support from the Texas Higher Education Coordinating Board Advanced Research Program. We also thank C. L. Chen and X. H. Chen for depositing the gold electrodes on the sample.

L. T. Wood's e-mail address is ltwood@uh.edu.

REFERENCES

1. R. W. Boyd, *Nonlinear Optics*, 2nd ed. (Academic, San Diego, 2003).
2. S. V. Popov, Y. U. Svirko, and N. I. Zheludev, *Susceptibility Tensors for Nonlinear Optics* (Institute of Physics, Bristol, UK, 1995).
3. A. F. Devonshire, "Theory of barium titanate—part I," Philos. Mag. **40**, 1040–1055 (1949).
4. A. F. Devonshire, "Theory of barium titanate—part II," Philos. Mag. **42**, 1065–1079 (1951).
5. A. F. Devonshire, "Theory of ferroelectrics," Adv. Phys. **3**, 85–130 (1954).
6. A. D. Franklin, "Ferroelectricity of barium titanate single crystals," Prog. Dielectr. **4**, 171–215 (1959).
7. W. J. Merz, "Ferroelectricity," Prog. Dielectr. **6**, 101–149 (1961).
8. E. T. Jaynes, *Ferroelectricity* (Princeton U. Press, Princeton, N.J., 1953).
9. H. D. Megaw, *Ferroelectricity in Crystals* (Methuen, London, 1957).
10. W. Känzig, "Ferroelectrics and antiferroelectrics," in Vol. 4 of Solid State Physics (Academic, New York, 1957), pp. 1–197.
11. F. Jona and G. Shirane, *Ferroelectric Crystals* (Pergamon, New York, 1962; reprint, Dover, New York, 1993).
12. J. C. Burfoot, *Ferroelectrics—An Introduction to the Physical Principles* (Van Nostrand, London, 1967).
13. J. Grindlay, *An Introduction to the Phenomenological Theory of Ferroelectricity* (Pergamon, Oxford, UK, 1970).
14. T. Mitsui, I. Tatsuzaki, and E. Nakamura, *An Introduction to the Physics of Ferroelectrics* (Gordon & Breach, New York, 1976).
15. M. E. Lines and A. M. Glass, *Principles and Applications of Ferroelectrics and Related Materials* (Clarendon, Oxford, UK, 1977).
16. J. C. Burfoot and G. W. Taylor, *Polar Dielectrics and Their Applications* (Macmillan, London, 1979).
17. V. M. Fridkin, *Photoferroelectrics* (Springer-Verlag, New York, 1979).
18. B. A. Strukov and A. P. Levanyuk, *Ferroelectric Phenomena in Crystals* (Springer-Verlag, New York, 1998).
19. D. Mayerhofer, "Transition to the ferroelectric state in barium titanate," Phys. Rev. **112**, 413–423 (1958).
20. W. Haas, R. Johannes, and P. Cholet, "Light beam deflection using the Kerr effect in single crystal prisms of $BaTiO_3$," Appl. Opt. **3**, 988–989 (1964).
21. V. E. Perfilova and A. S. Sonin, "The electro-optic properties of single crystals of barium titanate," Sov. Phys. Solid State **8**, 82–84 (1966).
22. A. S. Sonin and V. É. Perfilova, "Electro-optical properties of barium titanate in the paraelectric phase," Sov. Phys. Crystallogr. **14**, 419–420 (1969).
23. F.-S. Chen, "Modulators for optical communications," Proc. IEEE **58**, 1440–1457 (1970).
24. K. H. Hellwege, *Landolt-Börnstein, New Series III*, Vol. 2 (Springer-Verlag, Berlin, 1969).
25. K. H. Hellwege, *Landolt-Börnstein, New Series III*, Vol. 16 (Springer-Verlag, Berlin, 1981).
26. A. Yariv and P. Yeh, *Optical Waves in Crystals* (Wiley, New York, 2003).
27. M. J. Weber, *Handbook of Optical Materials* (CRC Press, Boca Raton, Fla., 2003).
28. R. L. Sutherland, *Handbook of Nonlinear Optics*, 2nd ed. (Marcel Dekker, New York, 2003).
29. J. F. Nye, *Physical Properties of Crystals* (Oxford U. Press, New York, 2001).
30. A. R. Johnston and J. M. Weingart, "Determination of the low-frequency linear electro-optic effect in tetragonal $BaTiO_3$," J. Opt. Soc. Am. **55**, 828–834 (1965).
31. R. M. A. Azzam and N. M. Bashara, *Ellipsometry and Polarized Light* (Elsevier, Amsterdam, 1987).
32. M. E. Drougard and D. R. Young, "Domain clamping effect in barium titanate single crystals," Phys. Rev. **94**, 1561–1564 (1954).
33. E. Burcsu, G. Ravichandran, and K. Bhattacharya, "Electro-mechanical behaviour of 90-degree domain motion in barium titanate single crystals," in *Smart Structures and Materials 2001: Active Materials: Behavior and Mechanics*, C. S. Lynch, ed., Proc. SPIE **4333**, 121–130 (2001).
34. E. Burcsu, "Investigations of large strain actuation in barium titanate," Ph.D. thesis (California Institute of Technology, Pasadena, Calif., 2001), http://etd.caltech.edu/etd/available/etd-10232001-192042/.
35. M.T.I. Corporation, www.mticrystal.com.
36. I. P. Kaminow, *An Introduction to Electro-optic Devices* (Academic, New York, 1974).
37. A. Yariv, *Optical Electronics in Modern Communications* (Oxford U. Press, New York, 1997).
38. R. D. Guenther, *Modern Optics* (Wiley, New York, 1990).
39. B. E. A. Saleh and M. C. Teich, *Fundamentals of Photonics* (Wiley, New York, 1991).
40. K. Iizuka, *Elements of Photonics* (Wiley, New York, 2002).
41. E. Hecht, *Optics*, 4th ed. (Pearson Addison Wesley, New York, 2001).
42. M. V. Klein and T. E. Furtak, *Optics*, 2nd ed. (Wiley, New York, 1986).
43. G. Fowles, *Introduction to Modern Optics*, 2nd ed. (Dover, New York, 1989).
44. M. Born and E. Wolf, *Principles of Optics*, 7th ed. (Cambridge U. Press, Cambridge, UK, 2002).
45. C. C. Davis, *Lasers and Electro-Optics* (Cambridge U. Press, Cambridge, UK, 1996).
46. M. V. Klassen-Neklyudova, *Mechanical Twinning of Crystals* (Consultants Bureau, New York, 1964).
47. M. Melnichuk and L. T. Wood, "Time-resolved optical transients in tetragonal $BaTiO_3$," J. Opt. Soc. Am. A (to be published).

Determining selected quadratic coefficients in noncentrosymmetric crystals

Mike Melnichuk and Lowell T. Wood

Department of Physics, University of Houston, Houston, Texas 77204-5005

Received May 25, 2005; revised October 11, 2005; accepted October 14, 2005; posted November 14, 2005 (Doc. ID 62378)

We present a systematic theoretical examination concerning the practical possibility of measuring components of the quadratic symmetry tensors for solid materials lacking inversion symmetry. We show that information concerning the quadratic effects in noncentrosymmetrical crystals can be obtained directly by methods that allow for the bypassing of the coexisting dominant linear effects. Here, we deal only with the particular case of the electro-optic effect; however, the results and conclusions are also valid for the elasto-optic effects. © 2006 Optical Society of America

OCIS codes: 190.3270, 160.2260, 260.1180, 160.1190, 230.4110.

1. INTRODUCTION

When a crystal is subjected to an externally applied vector stress field (electric or mechanical), it suffers a change in the internal structure, which in turn, causes a modification of its macroscopic physical properties. Theoretically, these properties are classified and labeled in a proper manner through concepts called physical parameters. The mathematical structures describing these parameters are tensors whose coefficients manifest certain relations of symmetry among themselves. The symmetry elements allow for an effective way of classifying all of the crystals into just a finite number of groups.

According to their macroscopic symmetry properties, crystals are divided into 32 point group classes. Out of these, 11 point groups have inversion symmetry; the crystals belonging to these classes are centrosymmetric. The other 21 point groups lack the inversion symmetry, making the corresponding crystals noncentrosymmetric.[1] Centrosymmetry means that the macroscopic physical properties of a crystal do not change with inversion in the direction of the externally applied vector stress field. In centrosymmetric crystals, the first-order (linear) effect is not present; the second-order (quadratic) effect is the principal one. By comparison, the general rule for the noncentrosymmetric crystals is that not all of their odd-rank tensors are zero, especially the first-rank ones; this makes their macroscopic properties very sensitive to inversions in the direction of the perturbing field. Of the 21 crystal point groups lacking inversion symmetry, 20 of them show a dominant linear effect in simultaneous coexistence with a quadratic one.[1,2] There is, however, one noncentrosymmetric point group (Cubic 432) for which the first-order effect is nonexistent because all the components (moduli) belonging to its first-rank tensor are zero; but this is not necessarily the case with all of its higher odd-rank tensors. In this particular case, being next in the order, the quadratic effect becomes the dominant one by default.

In this paper we will deal with the 20 noncentrosymmetric point groups for which the first- and second-order effects are present at the same time; in all of these cases, the quadratic effects are eclipsed by the linear ones. From a theoretical point of view, however, it can be shown that for 18 out of the 20 point groups, it is possible to measure directly selected components (coefficients) of the quadratic tensors of these crystals without having to deal with the dominant linear effects at all. This claim is based on properly understanding the practical advantages of a mathematical detail concerning a connection between the shape of the index ellipsoid (indicatrix) of a crystal and the externally applied vector field. This connection seems to have been overlooked by other authors, and in the following section, we will explain it carefully. We choose the electro-optic effect to be the representative case here, but the elasto-optic tensors have the same symmetry properties as the electro-optic tensors for each of these crystals. Finally, the validity of our claim has been already confirmed by the authors for the particular case of electro-optic effect on the tetragonal (4 mm) barium titanate ($BaTi0_3$) bulk single crystal at room temperature ($T = 23.5°C$).[3]

2. THEORY

This section is divided in two parts. In the first one we show theoretically how it is possible to avoid the first-order (Pockels) electro-optic effect to selectively measure elements of the second-order (Kerr) electro-optic tensors in noncentrosymmetric crystals. In the second part, we proceed systematically with a thorough analysis of all the groups of crystals lacking inversion symmetry and having a dominant Pockels effect in coexistence with the Kerr effect. Here, we show how the claim made in the Introduction can be applied to 18 out of the 20 symmetry point groups; the only exceptions are the symmetric point groups triclinic 1 and trigonal 3.

A. General Theoretical Analysis

The electro-optic effect is the change in the index ellipsoid (indicatrix) of a crystal when the crystal is subjected to an

1084-7529/06/050001-0/$15.00

externally applied electric field. For the most general case (a biaxial crystal), the equation of the initial index ellipsoid (initial indicatrix) at a zero electric field is given by

$$\frac{x_1^2}{n_1^2}+\frac{x_2^2}{n_2^2}+\frac{x_3^2}{n_3^2}=1. \tag{1}$$

With the application of an external electric field,

$$\mathbf{E}=E_1\hat{\mathbf{x}}_1+E_2\hat{\mathbf{x}}_2+E_3\hat{\mathbf{x}}_3, \tag{2}$$

the equation of the new index ellipsoid, in the same (x_1,x_2,x_3)-coordinate system, takes the new form

$$\frac{x_1^2}{n_1'^2}+\frac{x_2^2}{n_2'^2}+\frac{x_3^2}{n_3'^2}+\frac{2x_2x_3}{n_4'^2}+\frac{2x_1x_3}{n_5'^2}+\frac{2x_1x_2}{n_6'^2}=1. \tag{3}$$

To change from tensor to matrix notation, in Eq. (3), we used Nye's suffix abbreviation:[1]

$$(11)\rightarrow 1;\ (22)\rightarrow 2;\ (33)\rightarrow 3;\ (23),(32)\rightarrow 4;\ (13),(31)\rightarrow 5;\ (12),(21)\rightarrow 6.$$

With this notation, the Pockels and Kerr expressions connecting the new refractive indexes (n'), the initial ones (n), and the three components (E_1,E_2,E_3) of the applied electric field in the (x_1,x_2,x_3) system of coordinates can be written in a condensed form as

$$\frac{1}{n_i'^2}=\frac{1}{n_i^2}+r_{ij}E_j+R_{i(hl)}E_hE_l, \tag{4}$$

with $1/n_4=1/n_5=1/n_6=0$; $j,h,l=1,2,3$; $i,(hl)=1,2,\ldots,6$. With the matrix notation, Eq. (4) can be presented in a more explicit form as follows:

$$\begin{pmatrix}\frac{1}{n_1'^2}\\ \frac{1}{n_2'^2}\\ \frac{1}{n_3'^2}\\ \frac{1}{n_4'^2}\\ \frac{1}{n_5'^2}\\ \frac{1}{n_6'^2}\end{pmatrix}=\begin{pmatrix}\frac{1}{n_1^2}\\ \frac{1}{n_2^2}\\ \frac{1}{n_3^2}\\ 0\\ 0\\ 0\end{pmatrix}+\begin{bmatrix}r_{11}&r_{12}&r_{13}\\ r_{21}&r_{22}&r_{23}\\ r_{31}&r_{32}&r_{33}\\ r_{41}&r_{42}&r_{43}\\ r_{51}&r_{52}&r_{53}\\ r_{61}&r_{62}&r_{63}\end{bmatrix}\begin{pmatrix}E_1\\ E_2\\ E_3\end{pmatrix}$$

$$+\begin{bmatrix}R_{11}&R_{12}&R_{13}&R_{14}&R_{15}&R_{16}\\ R_{21}&R_{22}&R_{23}&R_{24}&R_{25}&R_{26}\\ R_{31}&R_{32}&R_{33}&R_{34}&R_{35}&R_{36}\\ R_{41}&R_{42}&R_{43}&R_{44}&R_{45}&R_{46}\\ R_{51}&R_{52}&R_{53}&R_{54}&R_{55}&R_{56}\\ R_{61}&R_{62}&R_{63}&R_{64}&R_{65}&R_{66}\end{bmatrix}\times\begin{pmatrix}E_1^2\\ E_2^2\\ E_3^2\\ E_2E_3\\ E_1E_3\\ E_1E_2\end{pmatrix}. \tag{5}$$

The r_{ij} and $R_{i(hl)}$ are the linear and the quadratic electro-optic tensor's components, respectively, and (hl) follows Nye's notation mentioned above.

The intersection of this new index ellipsoid [Eq. (3)] with the three planes x_2x_3, x_1x_3, and x_1x_2 will generate three sectional ellipses

$$x_px_q:\frac{x_p^2}{n_p'^2}+\frac{x_1^2}{n_q'^2}+\frac{2x_px_q}{n_m'^2}=1, \tag{6}$$

with their three corresponding pairs of principal (eigen)axes

$$\frac{1}{n_{m+}'^2}=\frac{\frac{1}{n_p'^2}\cos^2(\omega_m)-\frac{1}{n_q'^2}\sin^2(\omega_m)}{\cos(2\omega_m)}, \tag{7}$$

$$\frac{1}{n_{m-}'^2}=\frac{\frac{1}{n_p'^2}\cos^2(\omega_m)-\frac{1}{n_q'^2}\sin^2(\omega_m)}{\cos(2\omega_m)}, \tag{8}$$

or as functions of the n_m' indexes

$$\frac{1}{n_{m+}'^2}=\frac{1}{n_p'^2}+\frac{\tan(\omega_m)}{n_m'^2}, \tag{9}$$

$$\frac{1}{n_{m-}'^2}=\frac{1}{n_q'^2}-\frac{\tan(\omega_m)}{n_m'^2}; \tag{10}$$

here $p,q=1,2,3$ and $p<q$. The relation among p, q, and m follows the Nye index abbreviation: (pq), $(qp)\rightarrow m$; $m=4,5,6$. The three new index ellipses [Eq. (6)] are rotated with respect to the initial rectangular Cartesian system of coordinates (x_1,x_2,x_3) in the x_2x_3, x_1x_3, and x_1x_2 planes, with rotation angles ω_m given in a general way by the exact formula and its corresponding approximation up to the second order,

$$\tan(2\omega_m)=\frac{2/n_m'^2}{1/n_p'^2-1/n_q'^2}\cong\frac{2(r_{mj}E_j+R_{m(hl)}E_hE_l)}{(1/n_p^2-1/n_q^2)+(r_{pj}-r_{qj})E_j+(R_{p(hl)}-R_{q(hl)})E_hE_l}, \tag{11}$$

with the property $0<|\omega_m|<\pi/4$, for $m=4,5,6$.

B. Important Theoretical Observation

In Eqs. (6)–(8), the intersections of the sectional index ellipses with the x_1, x_2, and x_3 axes generate the refractive indices n_1', n_2', n_3'; this is independent of the order of ap-

proximation in the magnitude of the applied electric field. The indices of refraction mentioned above are related to the components of the field **E** through the following set of electro-optic equations:

$$\frac{1}{n_g'^2} = \frac{1}{n_g^2} + r_{gj}E_j + R_{g(hl)}E_hE_l. \tag{12}$$

In Eq. (12), note that if the experimental circumstances allow for the individual products $r_{gj}E_j=0$, with $g, j=1, 2, 3$, then the linear electro-optic effect will provide no contribution to the magnitude of the new refractive indices corresponding to the x_1, x_2, and x_3 directions.

A physical interpretation of the above statement is that any polarized light wave passing at normal incidence through any crystal in which the components of the applied electric field satisfy the condition $r_{gj}E_j=0$ for $g, j=1, 2, 3$, will have no contribution from the Pockels effect. For the above particular experimental configuration, the linear electro-optic effect cannot be detected. For other crystal structures, the above condition can be satisfied by changing either the crystal orientation or the direction of the applied electric field. Out of the 20 noncentrosymmetrical point symmetry classes showing both a Pockels and a Kerr effect, only 2 (triclinic 1, trigonal 3) do not satisfy this condition of selection for any experimental configuration.

3. EXPERIMENTAL SCHEMATIC

In Fig. 1 we present an experimental schematic of a optical modulator that can be used for measuring some of the Kerr coefficients in crystals lacking a center of symmetry. A similar experimental layout was previously used by the authors to successfully measure two off-diagonal Kerr coefficients (R_{21}, R_{31}) for the particular case of a $BaTiO_3$ single crystal in the tetragonal state (4 mm).[3] However, our optical modulator can be used, in principle, for the 18 out of 20 point group symmetry classes in which a Pockels and a Kerr effect are simultaneously present, with the first order electro-optic effect being the dominant one.

A. Theoretical Description of Optical Modulator Workings

As depicted in Fig. 1, the light coming from a very-low-power laser VLPL, passes through a linear polarizer LP, rotated by time-dependent angle $\theta(t)$ with respect to the horizontal. The polarized light then passes through the crystal sample CS, which has its cross-sectional index ellipse rotated by an angle ω_m ($m=4,5,6$) in the plane normal to the direction of the wave propagation (**k**); the change in shape and orientation of the index ellipsoid is caused by the electro-optic effect. Once it exits the back surface of the sample, the probing light wave carrying information about the crystal's indicatrix is split into two mutually orthogonal beams by a Wollaston prism WP, which is rotated by an angle ψ with respect to the horizontal. All angles are measured according to the trigonometric convention.

The formulas for the two modulated light intensities having mutually orthogonal polarizations are given by the two expressions

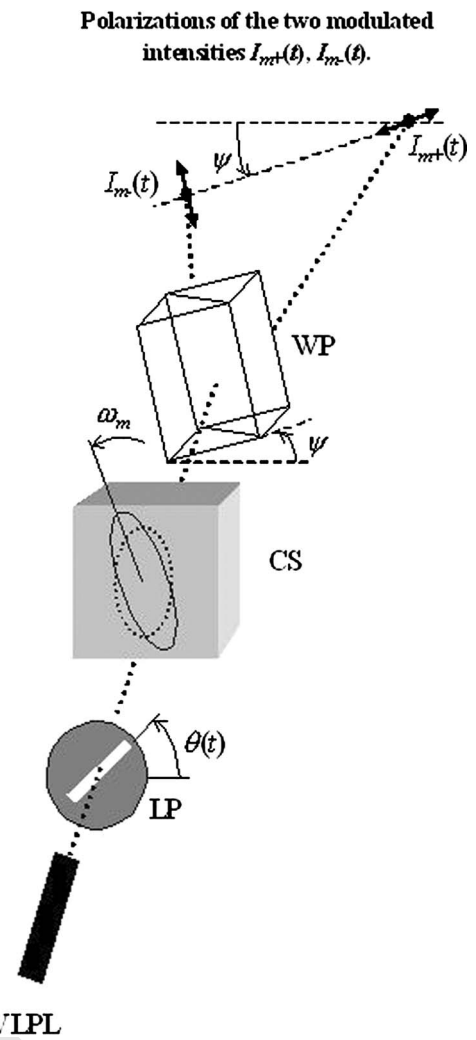

Fig. 1. Simple schematic of our optical amplitude modulator. The modulating system contains the following elements: very-low-power laser (VLPL), rotating linear polarizer (LP), crystal sample (CS), and a rotated Wollaston prism (WP). $\theta(t)$, ω_m ($m=4,5,6$), and ψ are the angles of rotation of the linear polarizer, the new sectional index ellipse, and the Wollaston prism, respectively; all angles are read according to the trigonometric convention. The angle of rotation of the linear polarizer is dependent on time.

$$I_{m+}(t) = A_{m+}^2[\theta(t),\psi] + A_{m+}[\theta(t),\omega_m] \times A_{m-}[\theta(t),\omega_m]\sin[2(\omega_m-\psi)]\sin^2\left(\frac{\Delta\varphi_m}{2}\right), \tag{13}$$

$$I_{m-}(t) = A_{m-}^2[\theta(t),\psi] - A_{m+}[\theta(t),\omega_m] \times A_{m-}[\theta(t),\omega_m]\sin[2(\omega_m-\psi)]\sin^2\left(\frac{\Delta\varphi_m}{2}\right), \tag{14}$$

with the amplitudes of the electromagnetic fields for an arbitrary set of variables ξ and ζ given by

$$A_{m+}(\xi,\zeta) = \frac{A_0}{2}[(T_{m+} + T_{m-})\cos(\xi - \zeta) + (T_{m+} - T_{m-})\cos(\xi + \zeta)], \quad (15)$$

$$A_{m-}(\xi,\zeta) = \frac{A_0}{2}[(T_{m+} + T_{m-})\sin(\xi - \zeta) - (T_{m+} - T_{m-})\sin(\xi + \zeta)]. \quad (16)$$

The terms

$$T_{m\pm} = T_{m\pm}(n'_{m\pm}) = \frac{4n'_{m\pm}}{(n'_{m\pm} + 1)^2} \quad (17)$$

and

$$\Delta\varphi_m = \Delta\varphi_m(n'_{m+}, n'_{m-}) = \frac{2\pi}{\lambda}(n'_{m+} - n'_{m-}) \quad (18)$$

are the single transmission coefficients of light at normal incidence and the optical retardation of the crystal sample, respectively; A_0 is the amplitude of the electromagnetic wave striking the linear polarizer.

B. General Description of the Experimental Procedure

The first experimental step should be to collect the values of the two mutually orthogonal intensities $[I_{0m+}(t), I_{0m-}(t)]$ for the virgin crystal sample during a complete rotation (2π rad) of the linear polarizer. These two intensities are the same as the ones provided in Eqs. (13)–(18) except for the effects due to the electro-optic phenomenon.

The next step consists of applying an electric field **E** and collecting the new values of the intensities $[I_{m+}(t), I_{m-}(t)]$. To make the experimental data independent of the effects of signal amplification, these intensities would be divided by the ones obtained for the crystal in its unperturbed initial state, giving the following relative intensities:

$$I^r_{m+}(t) = \frac{I_{m+}(t)}{I_{0m+}(t)}, \quad (19)$$

$$I^r_{m-}(t) = \frac{I_{m-}(t)}{I_{0m-}(t)}. \quad (20)$$

In the two expressions above, the terms in the numerator will behave the same as the terms in the denominator, with four visible exceptions at

$$\theta(t) = \omega_m + s\frac{\pi}{2}, \quad (21)$$

where $s=0, 1, 2, 3$. From the striking changes at these particular angles, it is possible to empirically extract the value of the angle ω_m ($m=4,5,6$). Once this angle is known, one can express n'_{m+} and n'_{m-} as functions of n'_p and n'_q from Eqs. (7)–(10). This set of refractive indices are the ones that contain some of the electro-optic coefficients to be determined. In crystals and experimental configurations for which the condition $r_{gi}E_j=0$ ($g,j=1,2,3$) applies, one can directly extract the values of at least two different Kerr coefficients. This is done by solving numerically for the two quadratic electro-optic coefficients in Eqs. (19) and (20); the values for the relative intensities $I^r_{m+}(t)$ and $I^r_{m-}(t)$ are gathered empirically from the experimental data. Now that the cross-sectional rotation angle ω_m and the two Kerr coefficients can be known, in principle one can make use of Eq. (11) to obtain extra information regarding the values of the electro-optic coefficients figuring at its numerator. These coefficients can be first-, second-, or even higher-order ones.

The specific details of the experimental procedure were provided by the authors in a previous paper,[3] in which a similar experimental design was used to determine for the first time two Kerr coefficients ($R_{12}=-3.5\pm0.3\times10^{-17}$ m^2/V^2, $R_{13}=-8.0\pm0.7\times10^{-17}$ m^2/V^2) of a tetragonal (4 mm) sample of bulk single $BaTiO_3$ crystal at room temperature ($T=23.5°C$). The precision of this method is at the 10% level for the $BaTiO_3$ results, and we see no reason for there to be substantial deviations of this level of precision for other materials.

4. DISCUSSION

In Tables 1–4 we present the electro-optic coefficients for all 18 noncentrosymmetrical crystal point groups that can be determined with the optical modulator we described above. In general, there can be a maximum of three electro-optic coefficients per experimental configuration; a new configuration corresponds to each row in the tables. By making use of the symmetries implicit in the electro-optic tensors for each particular crystal point group, one can obtain more than three coefficients per experimental layout. The fact that some crystal groups have tables smaller than others results from the limitation of the experimental configurations imposed by the theoretical condition of selection made in Subsection 2.B.

Independent of the order of the experimental readings, the Pockels coefficients relevant to each table were always calculated from Eq. (11) adapted for each respective situation. That means that these first-order terms could be determined either at the same time along with two other different Kerr coefficients or after the second-order coefficients were obtained separately from different experimental configurations that did not involve the respective Pockels terms. When a particular layout could allow, in principle, for the determination of electro-optic terms beyond second order, we mentioned that in the tables in an abbreviated manner as HOC [higher-order coefficient(s)].

The data set for each of the 18 crystal types, contained in the 4 tables, can be further divided into two parts: the part that presents all the experimental data that can be obtained through the consecutive application of just one individual component of the electric field and the part that considers the application of two perpendicular components of **E** at the same time. In obtaining the data pertaining to the second half, one needs to make use of the data gathered in the first half of each table; in this sense, the top half of each table has chronological priority over the bottom half for each individual point group. This is the reason that we mention only the newly gathered electro-optic coefficients in the second half; we assume the

Table 1. Selected Electro-optic Coefficients and Experimental Configurations for the Biaxial Noncentrosymmetric Crystals that Could Be Directly Measured with Our Optical Modulator[a]

E	k	Electro-optic Coefficients
	Monoclinic m	
E_2	$\mathbf{x}_1$	R_{22}, R_{32}, r_{42}
	$\mathbf{x}_2$	R_{12}, R_{32}, R_{52}
	$\mathbf{x}_3$	R_{12}, R_{22}, r_{62}
	Monoclinic 2	
E_1	$\mathbf{x}_1$	R_{21}, R_{31}, r_{41}
	$\mathbf{x}_2$	R_{11}, R_{31}, R_{51}
	$\mathbf{x}_3$	R_{21}, R_{22}, r_{61}
E_3	$\mathbf{x}_1$	R_{23}, R_{33}, r_{43}
	$\mathbf{x}_2$	R_{13}, R_{33}, R_{53}
	$\mathbf{x}_3$	R_{13}, R_{23}, r_{63}
E_1, E_3	$\mathbf{x}_1$	R_{25}, R_{35}
	$\mathbf{x}_2$	R_{15}, R_{35}, R_{55}
	$\mathbf{x}_3$	R_{15}, R_{25}
	Orthorhombic 222	
E_1	$\mathbf{x}_1$	R_{21}, R_{31}, r_{41}
	$\mathbf{x}_2$	R_{11}, R_{31}
	$\mathbf{x}_3$	R_{11}, R_{21}
E_2	$\mathbf{x}_1$	R_{22}, R_{32}
	$\mathbf{x}_2$	R_{12}, R_{32}, R_{52}
	$\mathbf{x}_3$	R_{12}, R_{22}
E_3	$\mathbf{x}_1$	R_{23}, R_{33}
	$\mathbf{x}_2$	R_{13}, R_{33}
	$\mathbf{x}_3$	R_{13}, R_{33}, r_{63}
E_2, E_3	$\mathbf{x}_1$	R_{44}
E_1, E_3	$\mathbf{x}_2$	R_{55}
E_1, E_2	$\mathbf{x}_3$	R_{66}
	Orthorhombic mm2	
E_1	$\mathbf{x}_1$	R_{21}, R_{31}
	$\mathbf{x}_2$	R_{11}, R_{31}, r_{51}
	$\mathbf{x}_3$	R_{11}, R_{21}
E_2	$\mathbf{x}_1$	R_{22}, R_{32}, r_{42}
	$\mathbf{x}_2$	R_{12}, R_{32}
	$\mathbf{x}_3$	R_{12}, R_{22}
E_1, E_2	$\mathbf{x}_3$	R_{66}

[a]The vector **k** represents the direction of incidence of the electromagnetic wave; it can be along any one of the $\mathbf{x}_1$, $\mathbf{x}_2$, or $\mathbf{x}_3$ Cartesian directions. **E** stands for the vector electric field applied on the crystal sample; its components along the $\mathbf{x}_1$, $\mathbf{x}_2$, and $\mathbf{x}_3$ directions are E_1, E_2, and E_3, respectively. The R's stand for Kerr coefficients and the r's for the Pockels ones. The initial refractive indices are assumed to be known.

Table 2. Selected Electro-optic Coefficients and Experimental Configurations for the Uniaxial Noncentrosymmetric Crystals that Could Be Directly Measured with Our Optical Modulator[a]

E	k	Electro-optic Coefficients
	Trigonal 32	
E_2	$\mathbf{x}_1$	$R_{22}, R_{11}, R_{32}, R_{31}, R_{42}, R_{41}, R_{56}$
	$\mathbf{x}_2$	$R_{12}, R_{21}, R_{32}, R_{31}, r_{52}, r_{41}$
	$\mathbf{x}_3$	$R_{12}, R_{21}, R_{22}, R_{11}, r_{62}, r_{21}, r_{11}$
E_3	$\mathbf{x}_1$	R_{23}, R_{13}, R_{33}
	$\mathbf{x}_2$	R_{13}, R_{23}, R_{33}
	$\mathbf{x}_3$	HOC
E_2, E_3	$\mathbf{x}_1$	$R_{24}, R_{14}, R_{65}, R_{44}, R_{55}$
	$\mathbf{x}_2$	R_{14}, R_{24}, R_{65}
	$\mathbf{x}_3$	R_{24}, R_{14}, R_{65}
	Trigonal 3m	
E_1	$\mathbf{x}_1$	$R_{21}, R_{12}, R_{31}, R_{32}, R_{41}, R_{42}$
	$\mathbf{x}_2$	$R_{11}, R_{22}, R_{31}, R_{32}, r_{51}, r_{42}$
	$\mathbf{x}_3$	$R_{11}, R_{22}, R_{21}, R_{12}, r_{61}, r_{22}, r_{12}$
	Hexagonal 622	
E_1	$\mathbf{x}_1$	$R_{21}, R_{12}, R_{31}, R_{32}, r_{41}, r_{52}$
	$\mathbf{x}_2$	$R_{11}, R_{22}, R_{31}, R_{32}$
	$\mathbf{x}_3$	$R_{11}, R_{22}, R_{21}, R_{12}$
E_2	$\mathbf{x}_1$	$R_{22}, R_{11}, R_{32}, R_{31}$
	$\mathbf{x}_2$	$R_{12}, R_{21}, R_{32}, R_{31}, r_{52}, r_{41}$
	$\mathbf{x}_3$	$R_{12}, R_{21}, R_{22}, R_{11}$
E_3	$\mathbf{x}_1$	R_{23}, R_{13}, R_{33}
	$\mathbf{x}_2$	R_{13}, R_{23}, R_{33}
	$\mathbf{x}_3$	HOC
E_2, E_3	$\mathbf{x}_1$	R_{44}, R_{55}
E_1, E_3	$\mathbf{x}_2$	R_{55}, R_{44}
E_1, E_2	$\mathbf{x}_3$	R_{66}
	Hexagonal 6mm	
E_1	$\mathbf{x}_1$	$R_{21}, R_{12}, R_{31}, R_{32}$
	$\mathbf{x}_2$	$R_{11}, R_{22}, R_{31}, R_{32}, r_{51}, r_{42}$
	$\mathbf{x}_3$	$R_{11}, R_{22}, R_{21}, R_{12}$
E_2	$\mathbf{x}_1$	$R_{22}, R_{11}, R_{32}, R_{31}, r_{42}, r_{51}$
	$\mathbf{x}_2$	$R_{12}, R_{21}, R_{32}, R_{31}$
	$\mathbf{x}_3$	$R_{12}, R_{21}, R_{22}, R_{11}$
E_1, E_2	$\mathbf{x}_3$	R_{66}

[a]Same as for Table 1. HOC [higher-order coefficient(s)] applies to cubic or higher-order moduli. The initial refractive indices are assumed to be known; the extraordinary indices of refraction are always considered along the x_3 axis.

other electron-optic coefficients that play a part to have been used from the first half of each of the tables. The experimental cases for which no new information could have been gained are not mentioned in the tables.

The initial refractive indices n_1, n_2, and n_3 were assumed to be known; the extraordinary indexes of refraction were always considered along the x_3 axis. The effects of inverse piezoelectricity, electrostriction, and light absorption in the crystal sample were neglected.

5. CONCLUSION

Armed with the confidence gained from the successful direct measurement of two distinct Kerr coefficients in the case of a tetragonal (4 mm) barium titanate ($BaTiO_3$)[3] single crystal, we extended the theoretical model to other crystal point groups. Although purely theoretical in nature, this paper shows in a systematic manner how it is possible to use an experimental design based on the working principles of a new optical modulator to determine Kerr and Pockels coefficients in a separate manner for 18 out of the 20 noncentrosymmetric crystal symmetry classes in which the two effects coexist; in these classes, the first-order (Pockels) effect is always the dominant one. The experimental design and procedure are similar to the ones we previously employed in the case of tetragonal $BaTiO_3$.

Table 3. Continuation of Table 2[a]

E	k	Electro-optic Coefficients
	Hexagonal –6m2	
E_1	$\mathbf{x}_1$	$R_{21}, R_{12}, R_{31}, R_{32}$
	$\mathbf{x}_2$	$R_{11}, R_{22}, R_{31}, R_{32}$
	$\mathbf{x}_3$	$R_{11}, R_{22}, R_{21}, R_{12}, r_{61}, r_{22}, r_{12}$
E_3	$\mathbf{x}_1$	R_{23}, R_{13}, R_{33}
	$\mathbf{x}_2$	R_{13}, R_{23}, R_{33}
	$\mathbf{x}_3$	HOC
E_1, E_3	$\mathbf{x}_2$	R_{55}, R_{44}
	$\mathbf{x}_3$	R_{66}
	Hexagonal 6	
E_1	$\mathbf{x}_1$	$R_{21}, R_{12}, R_{31}, R_{32}, r_{41}, r_{52}$
	$\mathbf{x}_2$	$R_{11}, R_{22}, R_{31}, R_{32}, r_{51}, r_{42}$
	$\mathbf{x}_3$	$R_{11}, R_{22}, R_{12}, R_{21}, r_{61}, R_{62}, R_{16}, R_{26}$
E_2	$\mathbf{x}_1$	$R_{22}, R_{11}, R_{32}, R_{33}, r_{42}, r_{51}$
	$\mathbf{x}_2$	$R_{12}, R_{21}, R_{32}, R_{31}, r_{52}, r_{41}$
	$\mathbf{x}_3$	$R_{12}, R_{21}, R_{22}, R_{11}, R_{62}, R_{61}, R_{16}, R_{26}$
E_1, E_2	$\mathbf{x}_3$	$R_{16}, R_{26}, R_{62}, R_{61}, R_{66}$
	Hexagonal –6	
E_3	$\mathbf{x}_1$	R_{23}, R_{13}, R_{33}
	$\mathbf{x}_2$	R_{13}, R_{23}, R_{33}
	$\mathbf{x}_3$	HOC
	Tetragonal 422, –42m	
E_1	$\mathbf{x}_1$	$R_{21}, R_{12}, R_{31}, R_{32}, r_{41}, r_{52}$
	$\mathbf{x}_2$	$R_{11}, R_{22}, R_{31}, R_{32}$
	$\mathbf{x}_3$	$R_{11}, R_{22}, R_{21}, R_{12}$
E_2	$\mathbf{x}_1$	$R_{22}, R_{11}, R_{32}, R_{31}$
	$\mathbf{x}_2$	$R_{12}, R_{21}, R_{32}, R_{31}, r_{52}, r_{41}$
	$\mathbf{x}_3$	$R_{12}, R_{21}, R_{22}, R_{11}$
E_3	$\mathbf{x}_1$	R_{23}, R_{13}, R_{33}
	$\mathbf{x}_2$	R_{13}, R_{23}, R_{33}
	$\mathbf{x}_3$	r_{63} (for –42 m)
E_2, E_3	$\mathbf{x}_1$	R_{44}, R_{55}
E_1, E_3	$\mathbf{x}_2$	R_{55}, R_{44}
E_1, E_2	$\mathbf{x}_3$	R_{66}

[a]Same as for Table 2.

Table 4. Completion of Table 2[a]

E	k	Electro-optic Coefficients
	Tetragonal 4mm	
E_1	$\mathbf{x}_1$	$R_{21}, R_{12}, R_{31}, R_{32}$
	$\mathbf{x}_2$	$R_{11}, R_{22}, R_{31}, R_{32}, r_{51}, r_{42}$
	$\mathbf{x}_3$	$R_{11}, R_{22}, R_{21}, R_{12}$
E_2	$\mathbf{x}_1$	$R_{22}, R_{11}, R_{32}, R_{31}, r_{42}, r_{51}$
	$\mathbf{x}_2$	$R_{12}, R_{21}, R_{32}, R_{31}$
	$\mathbf{x}_3$	$R_{12}, R_{21}, R_{22}, R_{11}$
E_1, E_2	$\mathbf{x}_3$	R_{66}
	Tetragonal 4, –4	
E_1	$\mathbf{x}_1$	$R_{21}, R_{12}, R_{31}, R_{32}, r_{41}, r_{52}$
	$\mathbf{x}_2$	$R_{11}, R_{22}, R_{31}, R_{32}, r_{51}, r_{42}$
	$\mathbf{x}_3$	$R_{11}, R_{22}, R_{21}, R_{12}, R_{61}, R_{62}$
E_2	$\mathbf{x}_1$	$R_{22}, R_{11}, R_{32}, R_{31}, r_{51}, r_{42}$
	$\mathbf{x}_2$	$R_{12}, R_{21}, R_{32}, R_{31}, r_{52}, r_{41}$
	$\mathbf{x}_3$	$R_{12}, R_{21}, R_{22}, R_{11}, R_{61}, R_{62}$
E_1, E_2	$\mathbf{x}_3$	R_{16}, R_{26}, R_{66}
	Anaxial Noncentrosymmetric	
E	**k**	Electro-optic Coefficients
	Cubic 23, –43 m	
E_1	$\mathbf{x}_1$	$R_{21}, R_{31}, R_{32}, R_{12}, R_{23}, R_{23}, r_{41}, r_{52}, r_{63}$
	$\mathbf{x}_2$	$R_{11}, R_{31}, R_{22}, R_{33}, R_{12}, R_{23}$
	$\mathbf{x}_3$	$R_{11}, R_{12}, R_{22}, R_{33}, R_{32}, R_{13}$
E_2	$\mathbf{x}_1$	$R_{22}, R_{32}, R_{11}, R_{33}, R_{21}, R_{13}$
	$\mathbf{x}_2$	$R_{12}, R_{32}, R_{31}, R_{23}, R_{21}, R_{13}, r_{52}, r_{41}, r_{63}$
	$\mathbf{x}_3$	$R_{12}, R_{22}, R_{31}, R_{23}, R_{11}, R_{33}$
E_3	$\mathbf{x}_1$	$R_{23}, R_{33}, R_{31}, R_{12}, R_{11}, R_{22}$
	$\mathbf{x}_2$	$R_{13}, R_{33}, R_{21}, R_{32}, r_{11}, R_{22}$
	$\mathbf{x}_3$	$R_{13}, R_{23}, R_{21}, R_{32}, R_{31}, R_{12}, r_{63}, r_{52}, r_{41}$
E_2, E_3	$\mathbf{x}_1$	R_{44}, R_{55}, R_{66}
E_1, E_3	$\mathbf{x}_2$	R_{55}, R_{44}, R_{66}
E_1, E_2	$\mathbf{x}_3$	R_{66}, R_{55}, R_{44}

[a]The initial refractive indices are assumed to be known; the extraordinary indices of refraction are always considered along the x_3 axis.

The major contribution of this paper is the fact that it shows the possibility of measuring many of the Kerr coefficients for crystals of which these second-order coefficients could have never been measured using the standard optical approaches to date.[4–12]

Another contribution is in regard to the Pockels effect. We show that it is possible to measure many of the first- and second-order electro-optic coefficients separately from one another. This allows for a more accurate determination of some of the Pockels coefficients because one can subtract the contributions due to the corresponding Kerr coefficients.

The last, but not least, contribution is the possibility of gaining some empirical information about the cubic- or higher-order electro-optic coefficients for some noncentrosymmetrical crystals within certain experimental configurations. To our knowledge, this has not been theoretically shown nor experimentally done before.

ACKNOWLEDGMENTS

The authors acknowledge support from the Texas Higher Education Coordinating Board Advanced Research Program.

L.T. Wood's e-mail address is ltwood@uh.edu.

*Current address: Department of Physics, University of Wisconsin - Milwaukee, Milwaukee, Wisconsin 53211.

REFERENCES

1. J. F. Nye, *Physical Properties of Crystals* (Oxford U. Press, 2001).
2. M. E. Lines and A. M. Glass, *Principles and Applications of Ferroelectrics and Related Materials* (Clarendon Press, 1977).
3. M. Melnichuk and L. T. Wood, "A method for measuring off-diagonal Kerr coefficients using polarized light transmission," J. Opt. Soc. Am. A **22**, 377–384 (2005).
4. I. P. Kaminow, *An Introduction to Electrooptic Devices* (Academic, 1974).

5. A. Yariv, *Optical Electronics in Modern Communications* (Oxford U. Press, 1997).
6. R. D. Guenther, *Modern Optics* (Wiley, 1990).
7. B. E. A. Saleh and M. C. Teich, *Fundamentals of Photonics* (Wiley, 1991).
8. K. Iizuka, *Elements of Photonics* (Wiley, 2002).
9. E. Hecht, *Optics*, 4th ed. (Pearson Addison-Wesley, 2001).
10. M. V. Klein and T. E. Furtak, *Optics*, 2nd ed. (Wiley, 1986).
11. G. Fowles, *Introduction to Modern Optics*, 2nd ed. (Dover, 1989).
12. M. Born and E. Wolf, *Principles of Optics*, 7th ed. (Cambridge U. Press, 2002).